Aust. J. Phys., 1983, **36**, 361–99

Survey of OH Masers at 1665 MHz. II* Galactic Longitude 340° to the Galactic Centre

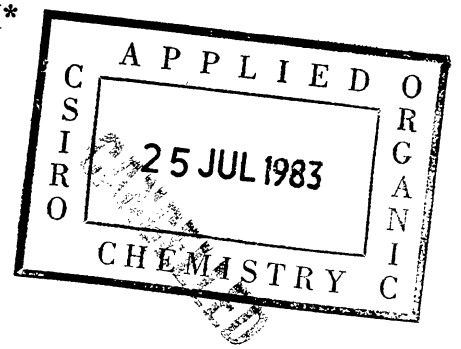

J. L. Caswell and R. F. Haynes

Division of Radiophysics, CSIRO,
P.O. Box 76, Epping, N.S.W. 2121.

Abstract

The galactic plane from longitude 340° through the galactic centre to longitude +2° has been searched for OH on the 1665 MHz transition. Forty-nine OH maser emission sources were detected and these have now been studied on all four OH ground-state transitions. Most of the masers are associated with regions of star formation (type I) while three may be examples of late-type stars (type II OH/IR) with unusually strong main-line emission.

Two especially interesting type I masers discovered are: OH 351·78−0·54, which is now the strongest OH maser known, with a peak intensity of nearly 1000 Jy ($\equiv 10^{-23}$ W m^{-2} Hz^{-1}), and OH 340·78−0·10, which displays an unusual velocity structure suggestive of a shell of emission.

Combining the present results with those of our earlier survey of longitudes 326° to 340° (Part I) doubles the number of well-studied type I OH sources. We have thus been able to improve our previous estimate of the luminosity function and have also now derived a galactic radial distribution extending to the galactic centre; this shows that while the inner 5 kpc of the Galaxy is generally deficient in type I OH masers, the immediate vicinity of the centre has a quite high density of such sources.

The conclusions of Part I were reassessed in the light of the new results. In the total sample of 85 type I sources six show accompanying strong 1720 MHz maser emission and nine show strong 1612 MHz maser emission; this significantly alters the statistics of Part I alone, which showed no 1720 MHz masers but six 1612 MHz masers. However, our earlier results regarding velocity structure, polarization and variability are generally corroborated; in particular, the present data reinforce our conclusions that a surprisingly large proportion of masers (including the exceptionally strong OH 351·78−0·54) have no closely related prominent HII region and quite likely pinpoint sites of the very early stages in star formation. The quite common occurrence of the masers within extensive OH clouds (as indicated by weak but spatially extended emission at 1612 or 1720 MHz) is also suggestive of dense molecular clouds in which star formation and HII region development are just beginning.

1. Introduction

The present search of the galactic plane for main-line OH sources extends our earlier survey (longitudes 326° to 340°: Caswell *et al.* 1980; hereafter referred to as Part I) to the galactic centre. It thus allows us to assess how OH masers are distributed throughout the Galaxy and in particular to discover whether the galactic centre differs greatly from regions further out.

Observations were made with a dual-channel parametric amplifier installed on the Parkes 64 m paraboloid. The system temperature was ~75 K on cold regions of

* Part I, *Aust. J. Phys.*, 1980, **33**, 639–69.

0004-9506/83/030361$02.00

sky. The Parkes 1024-channel correlator was used to obtain 512-point spectra for each circular polarization simultaneously. The intensity calibration is relative to Hydra A, for which a total flux density of 36 Jy was assumed (i.e. 18 Jy in each sense of circular polarization; the ratio of flux density to antenna temperature for *each* polarization is $0{\cdot}8\,\mathrm{Jy\,K^{-1}}$). The beamwidth to half-power is 12′ arc at 1665 MHz.

The Search: 1980 June 9–16

Observations were made on the 1665 MHz transition (with adopted rest frequency of 1665·401 MHz) covering a grid at $b = 0$ and $\pm 0^\circ{\cdot}2$, and spaced $0^\circ{\cdot}2$ in longitude from $l = 340^\circ$ through the galactic centre to $l = +2^\circ$. Positions with $|b| \geqslant 0^\circ{\cdot}4$ were observed where OH emission was detected at the edge of the original grid or where the continuum emission (see e.g. Haynes *et al.* 1978) extends significantly outside the $\pm 0^\circ{\cdot}3$ region—including a search at the positions of several discrete HII regions quite well separated from the plane.

The spectrum bandwidth analysed was 2 MHz wide and covered the radial velocity range -180 to $+180\,\mathrm{km\,s^{-1}}$ (relative to l.s.r.). The resolution (with uniform weighting) was 4·8 kHz ($0{\cdot}8\,\mathrm{km\,s^{-1}}$). Seven-minute integrations at each grid point combined with a 15 min reference yielded an r.m.s. noise level of $\sim 0{\cdot}1$ K (0·08 Jy) in each sense of polarization.

We note for comparison with our survey of longitudes 326° to 340° that the present search is symmetrical about zero velocity and covers a greater velocity range, but that the basic search was made only at 1665 MHz, whereas the 326°–340° region was searched on both main lines (i.e. 1665 *and* 1667 MHz).

Further Study: 1980 August 21–27, October 1–7 and 1981 January 28 to February 3

A more accurate position for each source was measured using a grid of observations with 6′ arc spacing centred on the approximate source position. On-source spectra were then obtained with higher frequency resolution, and usually a 0·2 MHz total bandwidth was used yielding (after Hanning weighting) a resolution of 0·8 kHz ≡ $0{\cdot}14\,\mathrm{km\,s^{-1}}$. Finally, observations were made at 1667, 1612 and 1720 MHz for most sources where no satisfactory previous data existed (at 1612 MHz many of the observations were already available from our 1612 MHz survey by Caswell *et al.* 1981). A complete survey of the region at 1667 and 1720 MHz has not been made; our observations at longitudes 326° to 340° suggest that, at most, one or two additional sources of type I might be present at 1667 MHz (with 1665 MHz emission below our sensitivity limit) and most likely no 1720 MHz sources (related to type I) over and above those detected at the positions of our 1665 MHz masers.

2. Results

(a) *OH Emission: Tabulation and Figures*

In Table 1 we list the main-line emission sources located in the survey region. Several had been found in earlier searches at the positions of strong HII regions and others during follow-up work to our 1612 MHz survey (Caswell *et al.* 1981). In column 1 we give the galactic coordinates; these, with the prefix OH, are subsequently used as the source name. Columns 2 and 3 give the equatorial coordinates and column 4 the positional uncertainty. Column 5 gives the range of

radial velocity over which there is significant OH emission; the centre of this range is usually a good estimate of the systemic velocity. The peak intensity on each of the ground-state transitions is given in columns 6–9, with R or L indicating whether right-hand or left-hand circular polarization is responsible for the peak signal. Any weak 1612 MHz emission that appears to be unpolarized and probably spatially extended is denoted IIc (following Caswell and Haynes 1975) and is often accompanied by 1720 MHz absorption (denoted abs). Likewise, weak IIa emission (at 1720 MHz) is often accompanied by 1612 MHz absorption (Haynes and Caswell 1977). Some of the main-line masers have been studied in earlier work, as referenced in column 10. Several of the masers can also be recognized amongst the survey data published by Turner (1979), but these were not positioned or studied in detail by Turner. Column 11 indicates whether an associated H_2O maser has been detected at the OH position; many of the positive (Y) detections are new results recently obtained with the Parkes radio telescope (Caswell *et al.* 1983, present issue p. 401). In column 12 we briefly describe the radio continuum in the vicinity, as depicted by the 5 GHz maps of Haynes *et al.* (1978). The kinematic distances in column 13 are based on the Schmidt (1965) model rotation curve using the OH velocity (see Section 3*a*).

The details of each source can best be seen in the line profiles of Figs 1–20 (where the order of the sources is of increasing longitude, with minor perturbations dictated by space-saving considerations).

Three of the sources have characteristics similar to OH/IR stars; however, they differ from the majority of such stars (cf. Caswell *et al.* 1981) in one important respect, namely, that the main-line emission (1665 and/or 1667 MHz) is stronger than or comparable with the 1612 MHz emission. In Fig. 20, which shows these three sources (OH 356·64−0·32, OH 358·23+0·11 and OH 358·66−0·05), we include the 1612 MHz emission profiles because of their importance to the source classification; in order to permit a single observation to cover the full velocity range of the emission, these three sources were observed with a lower velocity resolution than that used for the other sources.

(*b*) *Notes on Some Individual OH Sources*

Here we draw attention to unusual properties and remark on the following:

(1) Intensity variations in those sources monitored for several years.

(2) The presence of 1612 or 1720 MHz emission where it occurs.

(3) Pairs of right-hand and left-hand circularly (RHC and LHC) polarized emission components which are suggestive of the pattern arising from Zeeman splitting in a magnetic field (cf. Part I; note that in a 1 mG field ($\equiv 10^{-7}$ T) the separation of RHC and LHC components corresponds to 0·35 km s^{-1} at 1667 MHz and 0·59 km s^{-1} at 1665 MHz).

(4) Some unusual associations with continuum radio sources, IR objects etc.

OH 339·68−1·21 and OH 339·88−1·26 (Fig. 1). As is clear from their galactic latitudes, these sources lie outside the originally planned grid; furthermore they do not coincide with any distinct continuum emission (Haynes *et al.* 1978). They were discovered while making integrations intended as reference spectra of the receiver bandpass, in regions of sky expected to be free of OH emission or absorption. At the position of OH 339·68−1·21, sidelobe responses to the strongest features of OH 339·88−1·26 can be seen.

Table 1. OH main-line masers in the survey region of galactic longitudes 340° to 360° to 2°

(1) Galactic coordinates		(2) Position (1950)		(3) r.m.s. error	(4) Radial velocity[A]	(5) Intensity (and polarization) of peak[B]				(6) OH refs[C]	(7) H_2O?	(8) Radio continuum	(9) Kinematic distance[D]
l	b	R.A.	Dec.		(l.s.r.)	1665	1667	1612	1720				
°	°	h m s	° ′ ″	″	(km s^{-1})	(Jy)	(Jy)	(Jy)	(Jy)				(kpc)
339·68−1·21		16 47 26·2	−46 11 12	15	−28, −22	*7·5*(L)	6·1(L)	—	—		Y	Very weak	2·4, (16·4)
339·88−1·26		16 48 26·0	−46 03 41	15	−40, −27	*30·5*(R)	21·9(R)	—	—		Y	None?	3·1, (15·7)
340·06−0·25		16 44 36·9	−45 16 27	15	−58, −48	*12·0*(R)	9·7(R)	—	—	RCG	Y	HII	4·6, 14·2
340·78−0·10		16 46 38·0	−44 37 23	15	−108, −89	*11·8*(R)	*5·5*(R)	—	1·0(L)			Very weak	9·4
341·21−0·21		16 48 40·6	−44 21 54	15	−42, −36	*8·7*(R)	2·2(R)	—	—		Y	Discrete source	3·6, 15·3
341·27+0·07		16 47 39·6	−44 08 39	20	−73	*2·0*(L)	—	—	—			None	6·3, 12·7
343·12−0·06		16 54 42·6	−42 47 34	15	−37, −27	*110*(L)	12·0(L)	23(R, L)	—	CHGM	Y	Edge extended HII	3·2, 15·9
343·93+0·12		16 56 39·1	−42 02 58	16	+10, +14	*5·4*(L)	abs	—	—			Weak extended	∼0, 19·5
344·22−0·57		17 00 33·8	−42 14 35	19	−32, −29	*2·3*(R)	9·6(R)	abs	IIa		Y	Compact HII	3·4, 15·8
344·41+0·05		16 58 34·0	−41 43 15	24	−65	*2·9*(L)	abs	IIc	abs	CHGM		Edge compact HII	6·3, 12·7
344·58−0·02		16 59 27·1	−41 37 42	15	−11, +2	*18·6*(R)	9·4(L)	—	—		Y	Edge, weak extended	0·7, 18·6
345·00−0·22		17 01 39·3	−41 24 50	15	−33, −24	*3·6*(L)	2·2(R)	IIc	*43*(L)		Y	Edge extended source	3·2, 16·1
345·01+1·79		16 53 19·0	−40 09 46	15	−31, −19	*19·2*(L)	5·5(L)	—	—		Y	Edge large HII	3·0, (16·4)
345·4	−0·9	17 05 58	−41 32 50	60	−19, −17	*1·5*(L)	abs	IIc	abs	HCG	Y	Strong HII	2·3, (17·1)
345·51+0·35		17 00 54·7	−40 39 59	15	−25, −12	*15·6*(R)	10·4(R)	IIc	abs	RCG	Y	HII	2·1, 17·3
345·70−0·09		17 03 21·5	−40 47 01	15	−11, −3	*10·2*(R)	12·3(R)	9·2(R, L)	—	RCG	Y	Edge HII	1·0, 18·4
346·48+0·13		17 04 55·8	−40 01 40	16	−17, −7	*3·3*(L)	—	—	—			Edge compact HII	1·8, 17·6
347·63+0·15		17 08 23·9	−39 05 50	15	−99, −92	*8·6*(L)	*3·2*(R)	*2·9*(R)	—	RCG	Y	Strong extended HII	9·7
347·87+0·01		17 09 41·7	−38 59 13	16	−34, −30	*6·4*(L)	—	—	—			Compact HII	4·3, 15·3
348·55−0·97		17 15 51·4	−39 00 30	30	−23, −10	*4·5*(R)	1·1(L)	—	*6·9*(L)	CHG	Y	Strong HII	2·5, (17·1)
348·73−1·06		17 16 46	−38 54 36	45	−17, −6	*1·5*(R)	—	IIc	abs	CHG	Y	Strong HII	1·8, (17·8)
348·89+0·09		17 12 25·7	−38 06 50	16	−75, −72	*3·3*(R)	—	—	—		Y?	None	8·9, 10·7
348·89−0·19		17 13 35·9	−38 16 37	20	+2, +11	*1·5*(R)	0·5(R)	—	—		Y	Compact 0·4 Jy source	∼0, 21·1
349·07−0·01		17 13 25·6	−38 01 31	16	+14, +16	*2·4*(R)	—	—	—	CR	Y	HII	∼0, 23·2
349·09+0·11		17 12 58·4	−37 56 20	18	−91, −79	*3·0*(L)	0·8(R)	—	—	RCG	Y	HII	9·8

1983AuJPh..36..361C

Table 1 (*Continued*)

(1)	(2)	(3)	(4)	(5)	(6)	(7)	(8)	(9)	(10)	(11)	(12)	(13)
350·02+0·43	17 14 24·1	−37 00 04	25	−34, −33	*1·4*(L)	—	—	—		Y	Compact 0·6 Jy source	5·0, 14·7
350·11+0·09	17 16 02·3	−37 07 00	15	−77, −65	*69*(R)	3·9(R)	—	—		Y	HII	9·8
351·16+0·70	17 16 36·3	−35 54 57	15	−16, −3	*70*(R)	136(R)	—	—	WWDL	Y	NGC 6334B(S)	1·7, (18·1)
351·41+0·64	17 17 32·1	−35 44 15	15	−14, −6	*249*(L)	47(L)	—	42(L)	WWDL	Y	NGC 6334A(N)	1·9, (17·9)
351·58−0·35	17 22 02·5	−36 09 51	16	−100, −88	*9·2*(R)	0·3(R, L)	IIc	abs	CHGM	Y	Compact HII	9·9
351·78−0·54	17 23 20·9	−36 06 46	15	−29, +8	*960*(L)	*11·7*(L)	IIc	abs	CH	Y	0·3 Jy source	2·2, 17·6
352·16+0·21	17 21 24·2	−35 22 11	19	−42	*2·5*(L)	—	—	—			None	7·0, 12·8
352·51−0·15	17 23 49·5	−35 17 09	17	−56, −45	*2·6*(L)	2·8(R)	—	—		Y	None? see text	8·0, 11·8
353·41−0·36	17 27 06·0	−34 39 20	14	−21, −19	*8·7*(L)	abs	IIc	*21*(L)	CR	Y	HII	4·5, 15·3
353·45+0·54	17 23 35·7	−34 06 54	19	−46, −36	*1·3*(R, L)	—	1·3(R, L)	—		Y	Complex emission	8·4, 11·4
354·61+0·48	17 26 59·0	−33 11 35	15	−18, −12	*8·2*(R)	4·5(R)	1·1(R)	—	CHGM	Y	HII	4·2, 15·7
355·34+0·15	17 30 12·0	−32 45 54	15	+14, +22	*16·4*(R)	0·3(R, L)	—	—	CR	Y	HII	∼0, (>20)
356·64−0·32	17 35 24·4	−31 55 40	30	−28, +13	1·1(R)	*2·3*(R)	*1·3*(R)	—	CHGM	Y	None	2·5, 17·4
356·66−0·27	17 35 14·9	−31 53 17	19	−55, −53	*2·9*(L)	2·4(R)	IIc	—			None	10
358·23+0·11	17 37 40·6	−30 21 39	17	−33, +20	*3·2*(R)	3·2(L)	1·4(R, L)	—		Y	None	10
358·66−0·05	17 39 22·4	−30 04 35	20	−33, +29	*3·3*(L)	1·1(L)	2·3(R, L)	—	CHGM	Y	Galactic centre bulge	6·0, 14·0
359·14+0·03	17 40 14·6	−29 38 12	15	−7, +1	*8·4*(L)	4·2(R)	—	IIa	CF	Y	Galactic centre bulge	5·0, 15·0
359·43−0·10	17 41 28·3	−29 27 04	15	−54, −50	*8·0*(L)	0·8(L)	abs	IIa		Y	HII	10±1
359·62−0·25	17 42 30·0	−29 22 31	26	+19, +27	*2·7*(R)	1·8(R)	—	—		Y	HII	10±1
359·97−0·46	17 44 09·8	−29 10 55	15	+13, +18	*15·5*(L)	abs	IIc	abs		Y	Galactic centre bulge	10±1
0·37+0·04	17 43 10·04	−28 35 01	23	+30, +39	*3·0*(R)	3·3(L)	—	—		Y	Galactic centre bulge	10±1
0·54−0·85	17 47 04·1	−28 54 01	17	+4, +20	2·3(R)	*2·9*(R)	abs	IIa	GW	Y	Compact HII	∼2, (∼18)
0·66−0·04	17 44 10·6	−28 22 42	20	+48, +77	*128*(L)	25(L)	∼5	25(R)	MRGB	Y	Sgr B2 HII	10±1
2·14+0·01	17 47 29·0	−27 05 01	17	+58, +66	*5·0*(R)	*2·0*(L)	—	—		Y	None	8·9, 11·1

[A] Range of radial velocity over which emission is detectable.

[B] Epoch 1980 October or 1981 February. Transition(s) used for position determination given in italics. IIc and IIa refer to weak emission as discussed in Section 2*a*.

[C] RCG, Robinson *et al.* (1974); CHGM, Caswell *et al.* (1981); HCG, Haynes *et al.* (1976); CHG, Caswell *et al.* (1977); CR, Caswell and Robinson (1974); WWDL, Weaver *et al.* (1965); CH, Caswell and Haynes (1980); CF, Cohen and Few (1976); GW, Gardner and Whiteoak (1975); MRGB, McGee *et al.* (1965).

[D] Near and far distances are given; where evidence favours one of these, the less likely value is enclosed in parentheses.

OH340·06−0·25 (*Fig. 2*). See Part I for a discussion of earlier observations and evidence of intensity variability. Data now span more than a decade (back to 1970); over the past four years changes have been small.

OH340·78−0·10 (*Fig. 2*). The velocity structure shows two regions of emission separated by $\sim 14\ \mathrm{km\,s^{-1}}$ (and a total range of $\sim 20\ \mathrm{km\,s^{-1}}$). This superficially resembles the 1612 MHz OH/IR late-type stars but in the present case there is no detectable 1612 MHz emission. Furthermore, there is weak 1720 MHz emission (not found in any of the known OH/IR stars). The source is clearly of considerable importance in view of its 'difficult to classify' nature. The velocity structure is likely to be the result of an expanding or a contracting shell. Continuum emission is not evident. The large negative mean velocity indicates a source position near the tangential point; thus the kinematic distance is well defined (and large) and the intrinsic luminosity is similarly well defined (and large).

OH341·21−0·21 (*Fig. 2*). Both the 1665 and 1667 MHz profiles are suggestive of Zeeman splitting ($3{\cdot}5\ \mathrm{km\,s^{-1}}$ at 1665 MHz and $2{\cdot}2\ \mathrm{km\,s^{-1}}$ at 1667 MHz) in a line-of-sight magnetic field of 6 mG.

OH343·12−0·06 (*Fig. 3*). The emission at both 1665 and 1667 MHz is highly polarized, almost 100% LHC, perhaps indicating strong gradients of magnetic field and velocity (see Section 3*c*). In contrast, the 1612 MHz emission (Caswell *et al.* 1981) shows essentially no circular polarization.

OH344·22−0·57 (*Fig. 4*). Note the quite rare situation whereby 1667 MHz emission has a larger intensity than 1665 MHz emission.

OH344·41+0·05 (*Fig. 5*). This source is embedded in an extended absorbing OH cloud which shows weak type IIc 1612 MHz emission (Caswell *et al.* 1981).

OH344·58−0·02 (*Fig. 4*). At both 1665 and 1667 MHz the spectrum shows essentially continuous emission spread over $\sim 12\ \mathrm{km\,s^{-1}}$. However, there are a large number of peaks and the emission is thus clearly composed of a very large number of individual overlapping features, making it an interesting candidate for investigation by VLBI mapping techniques.

OH345·00−0·22 (*Fig. 5*). The maser is embedded in an extensive OH cloud which gives rise to broad main-line absorption. A strong 1720 MHz maser is also present.

OH345·01+1·79 (*Fig. 5*). This source is situated in a large nearby HII region displaced from the galactic plane.

OH345·4−0·9 (*Fig. 6*). This source was first discovered by Haynes *et al.* (1976). The emission is still similar to that seen in 1976. The 1667 MHz profile shows only absorption from an extended cloud of OH and from this the underlying absorption at 1665 MHz can be estimated (by assuming it to be $\frac{5}{9}$ times the value at 1667 MHz, as is appropriate for an optically thin cloud); the 1665 MHz emission intensity of 1·5 Jy (see Table 1) has been measured relative to the underlying absorption. The extended absorbing cloud shows weak type IIc emission at 1612 MHz and corresponding anomalously strong 1720 MHz absorption.

Figs 1–19. Spectra of OH main-line masers. The continuous thick curve denotes the right-hand sense of circular polarization and the thin (dashed) curve denotes the left-hand sense. In all figures the intensity scale refers to one sense of polarization so that the total intensity is the sum (not the mean) of the intensities in each polarization. The velocity resolution is $0{\cdot}14\ \mathrm{km\,s^{-1}}$ (0·8 kHz). Some profiles were observed in October 1980 and the remainder in February 1981.

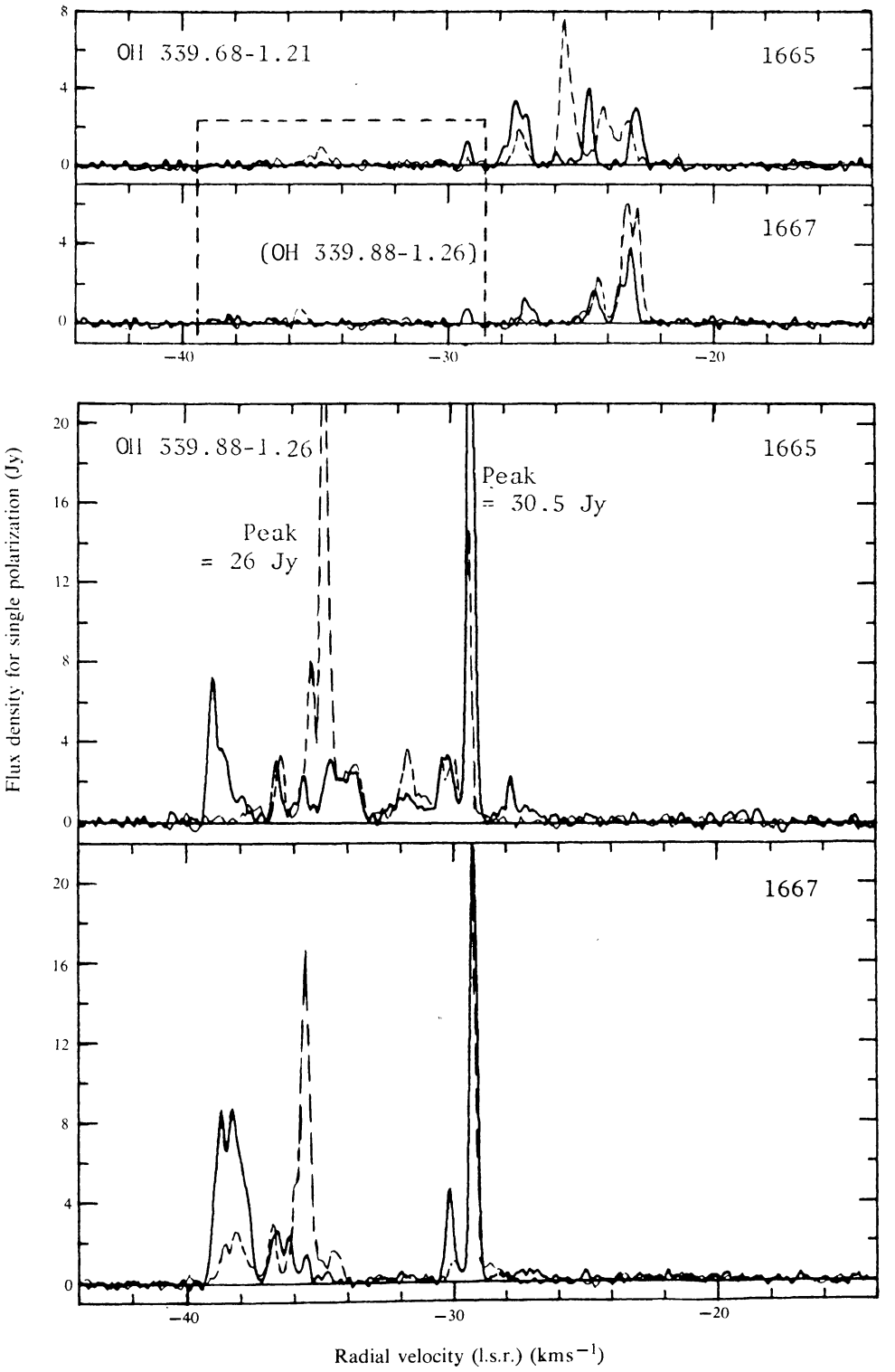

Fig. 1

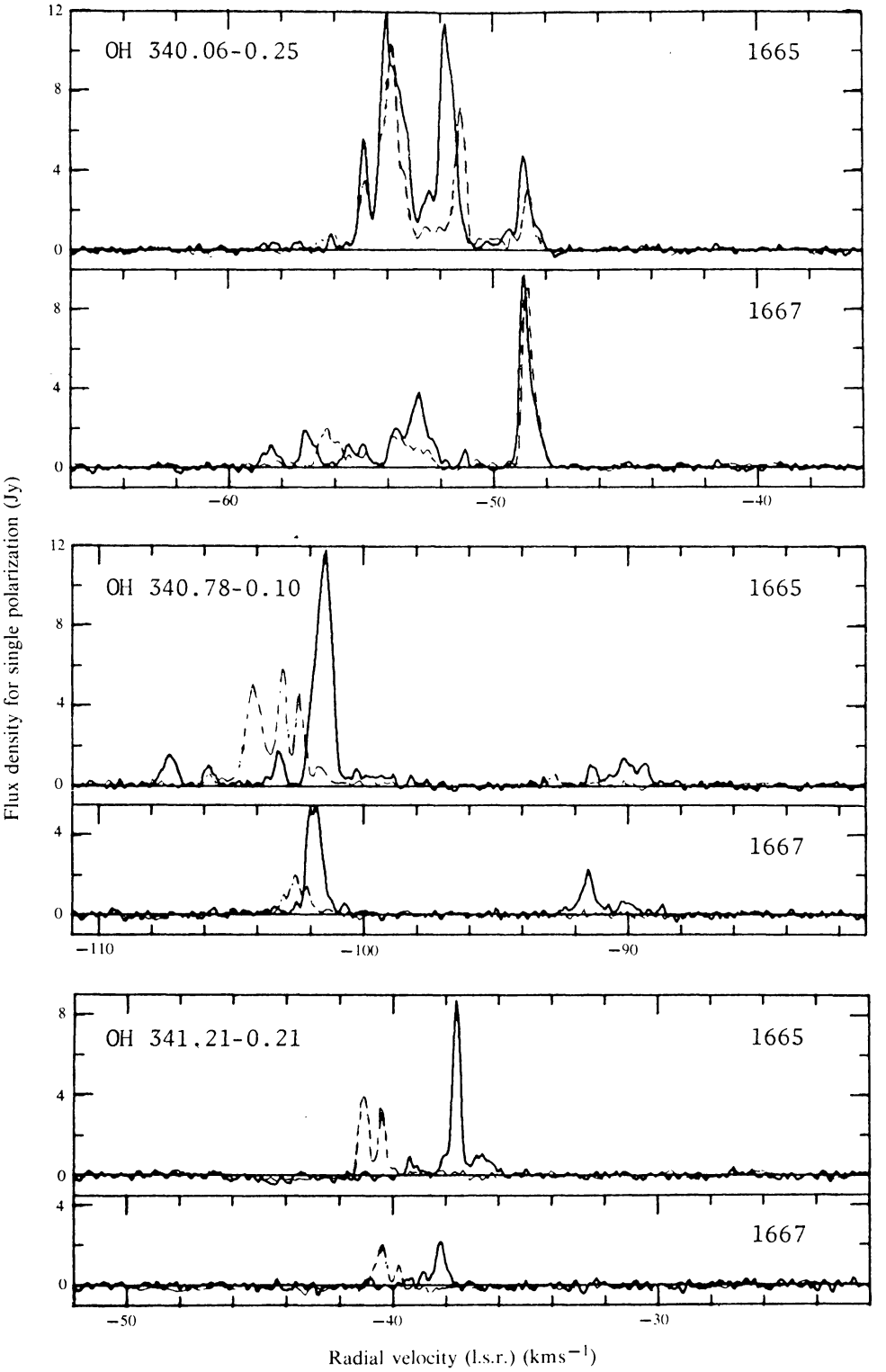

Fig. 2

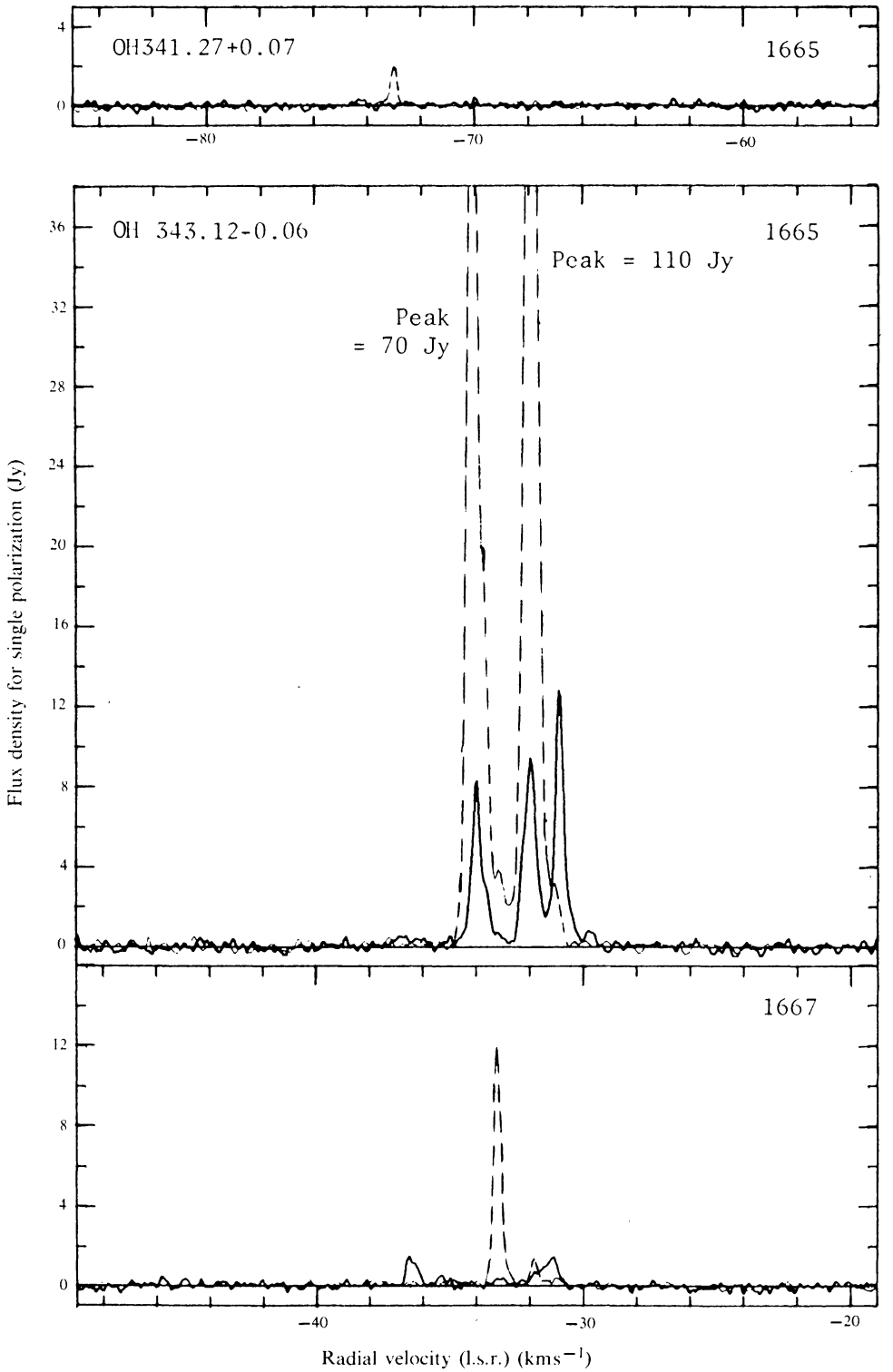

Fig. 3

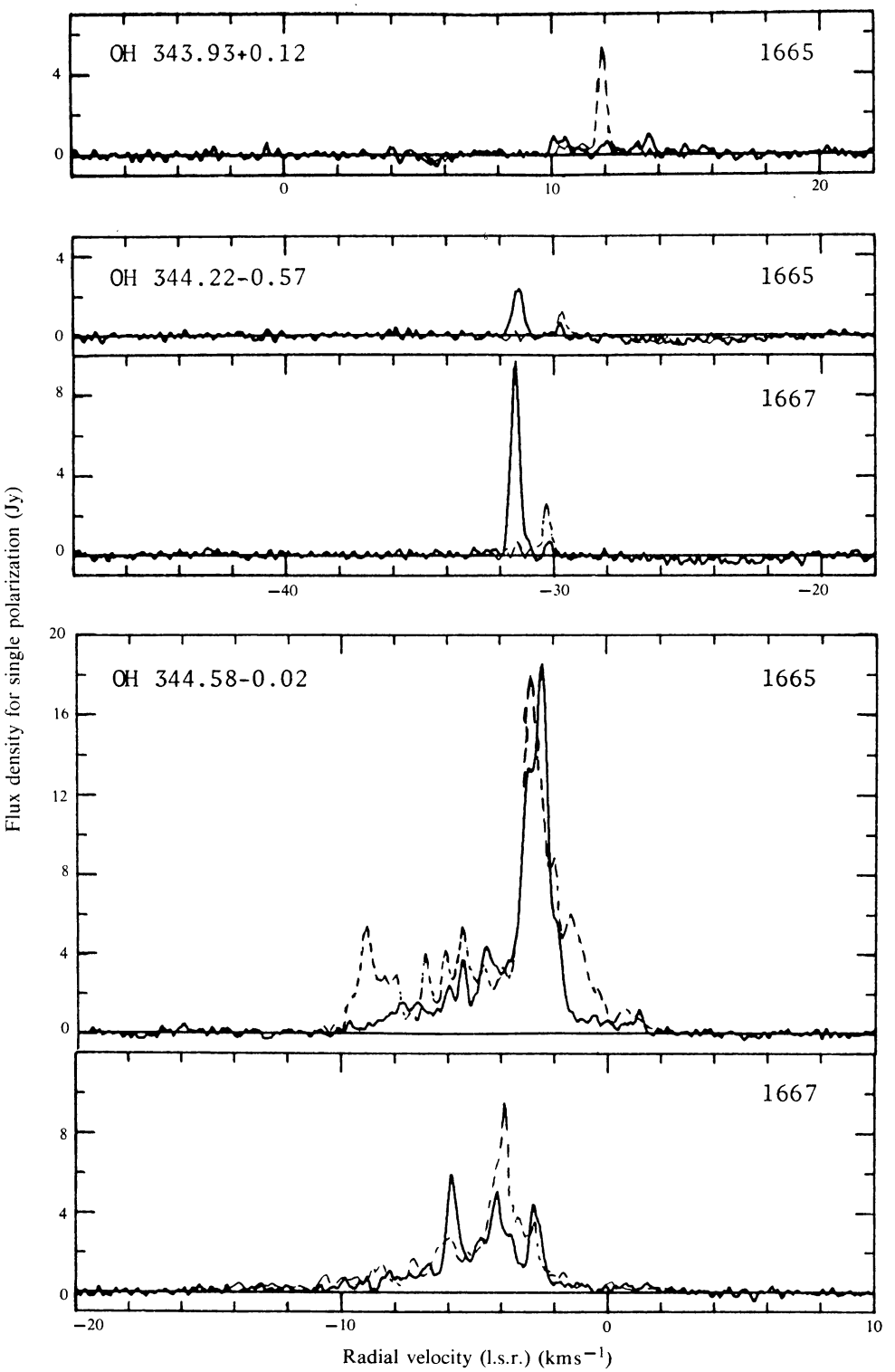

Fig. 4

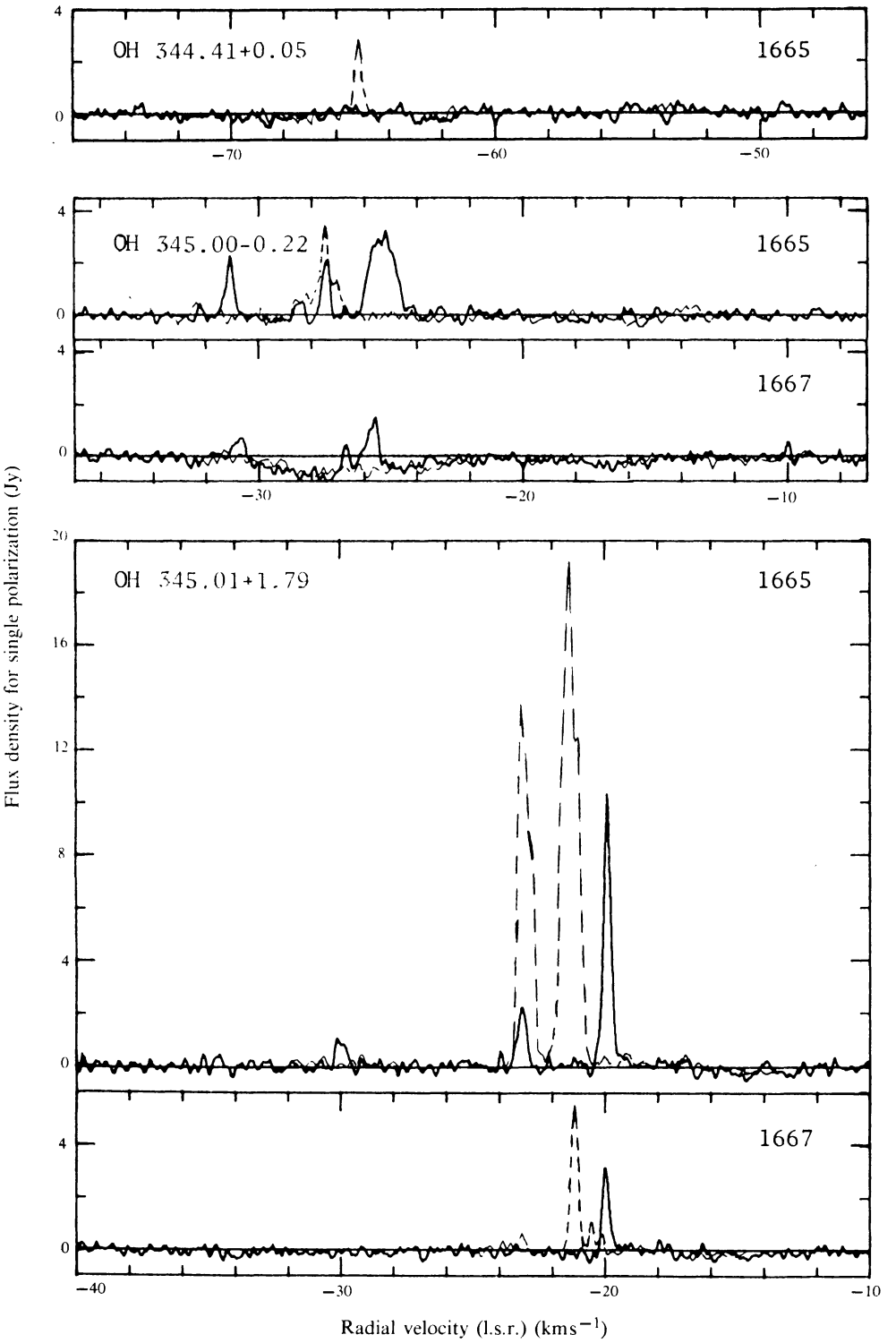

Fig. 5

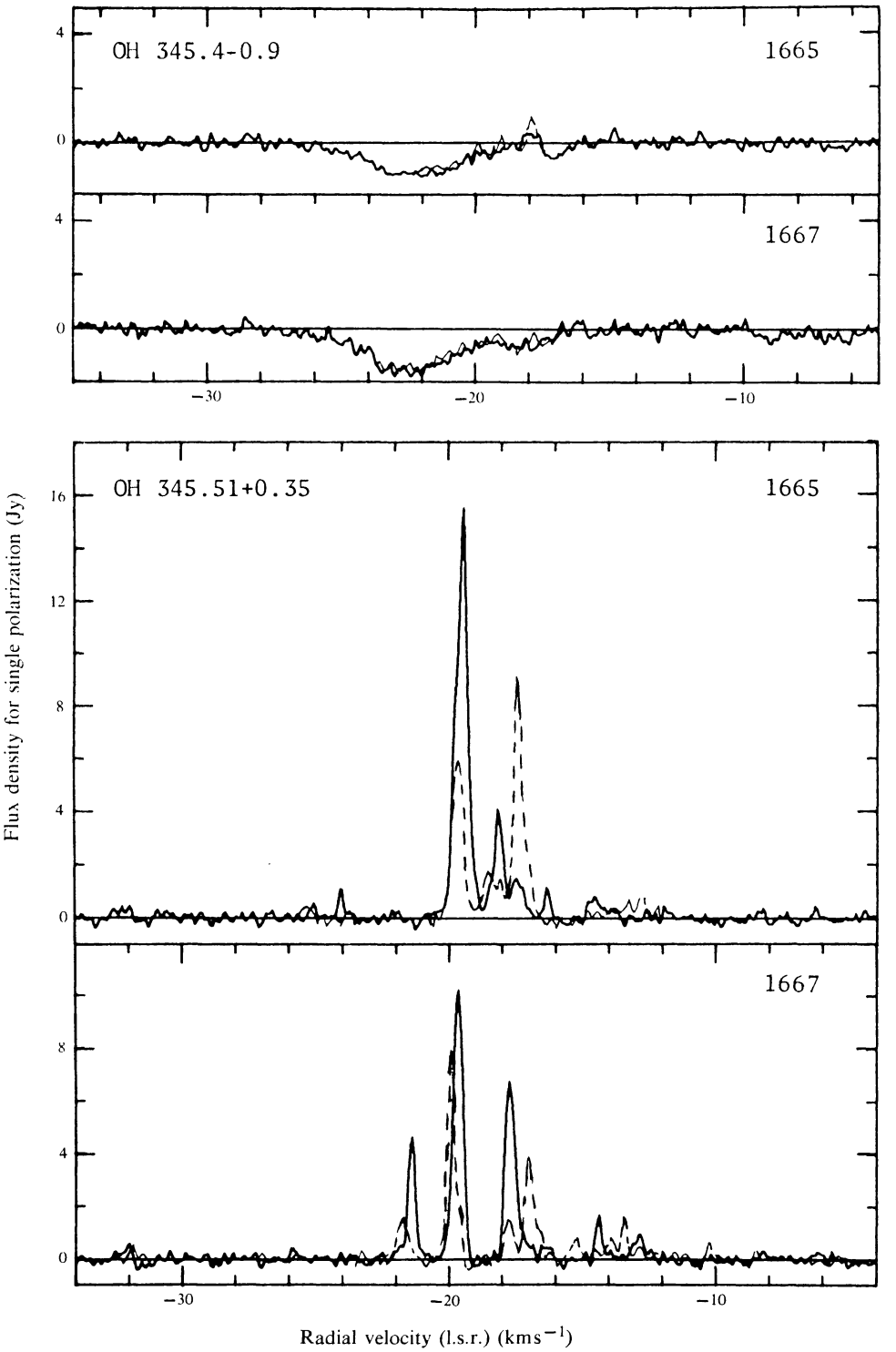

Fig. 6

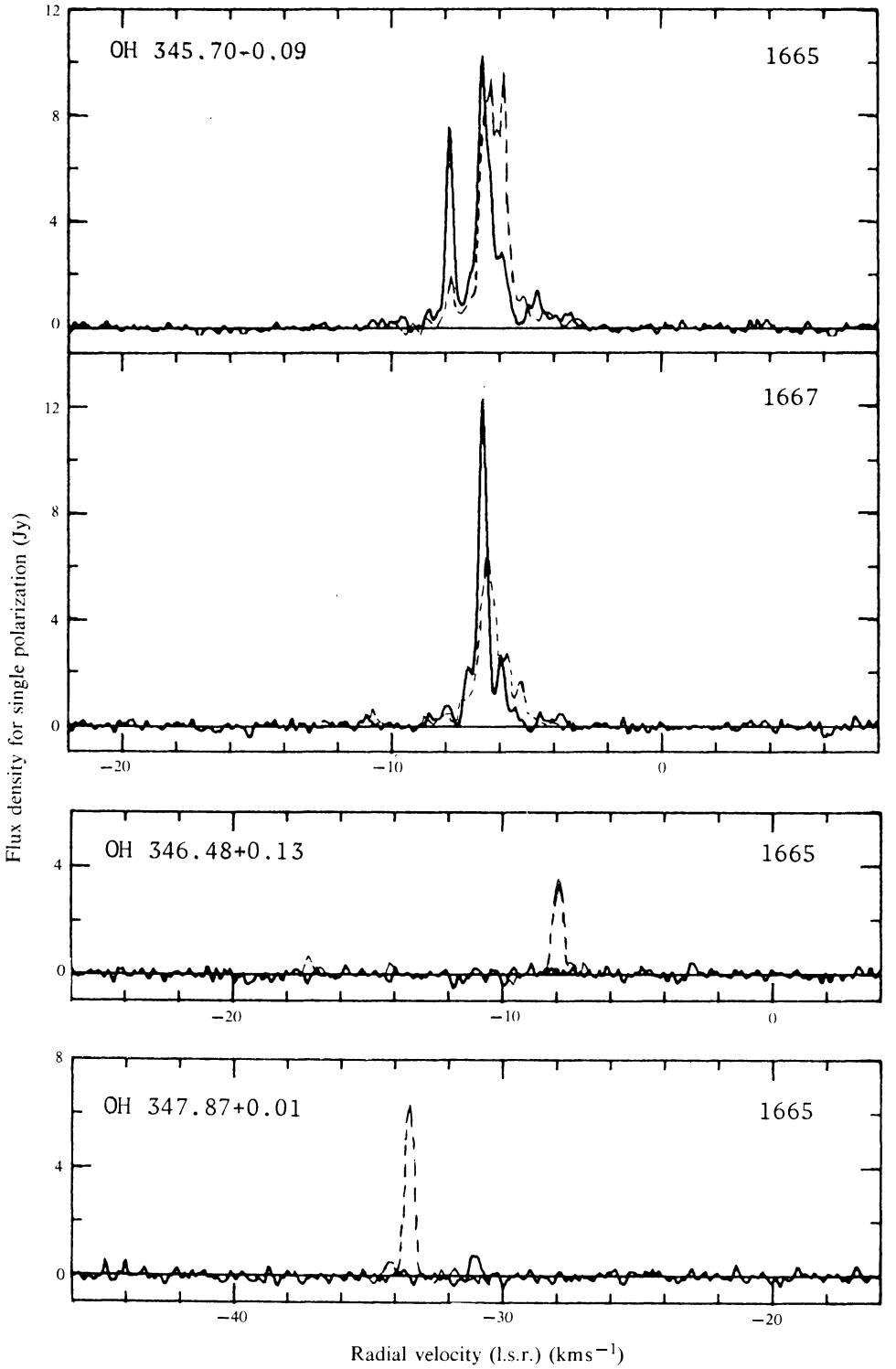

Fig. 7

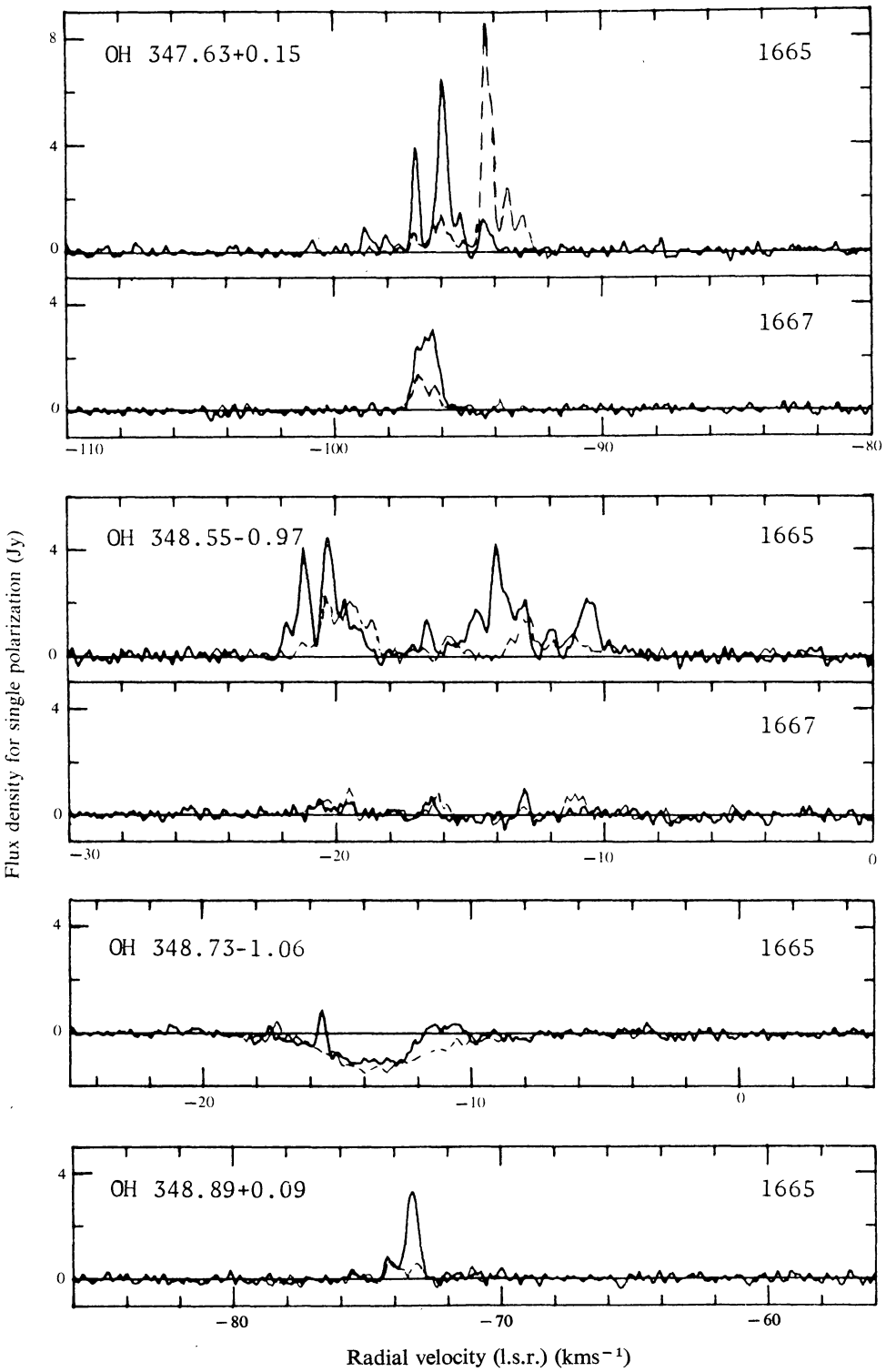

Fig. 8

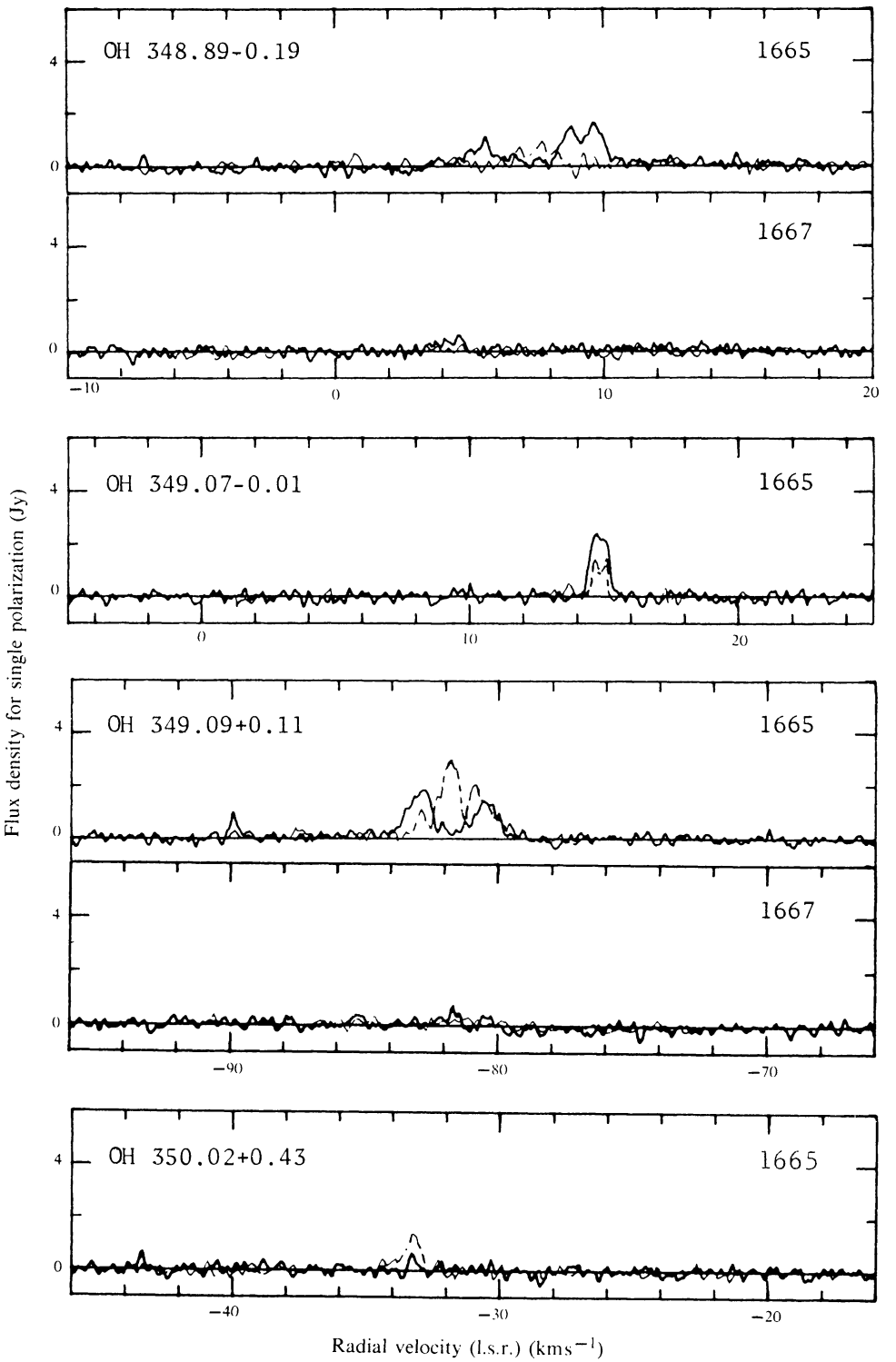

Fig. 9

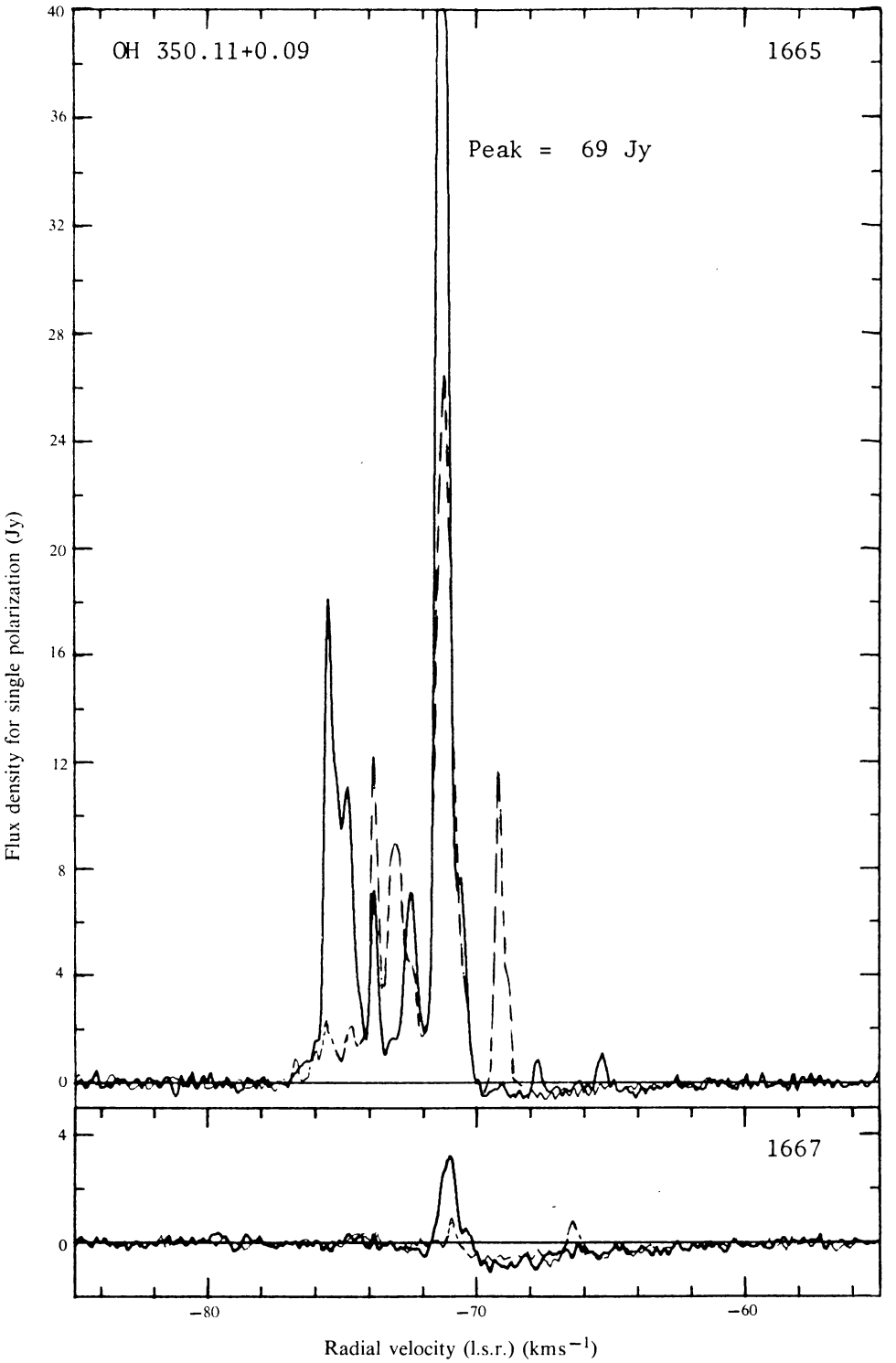

Fig. 10

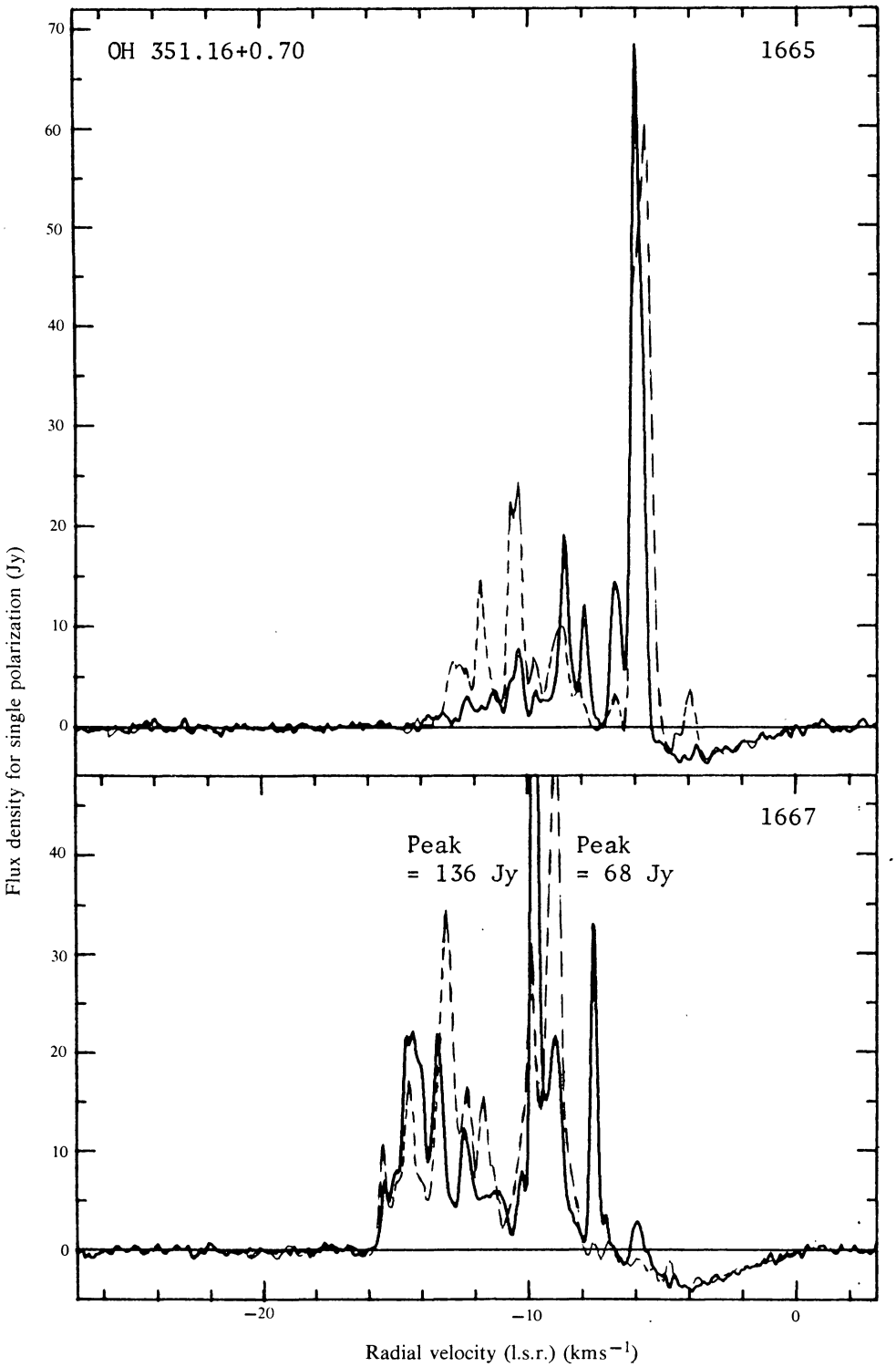

Fig. 11

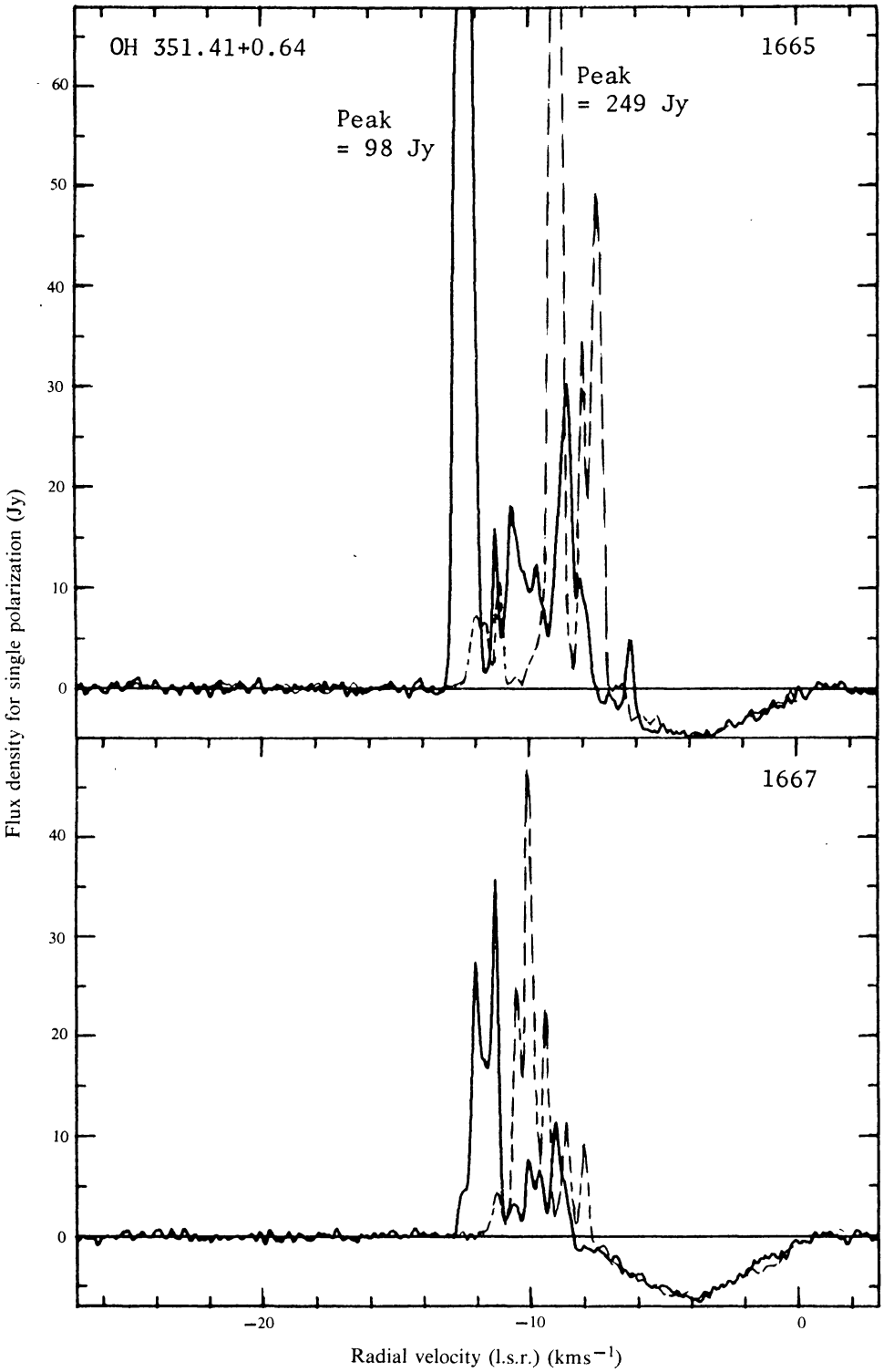

Fig. 12

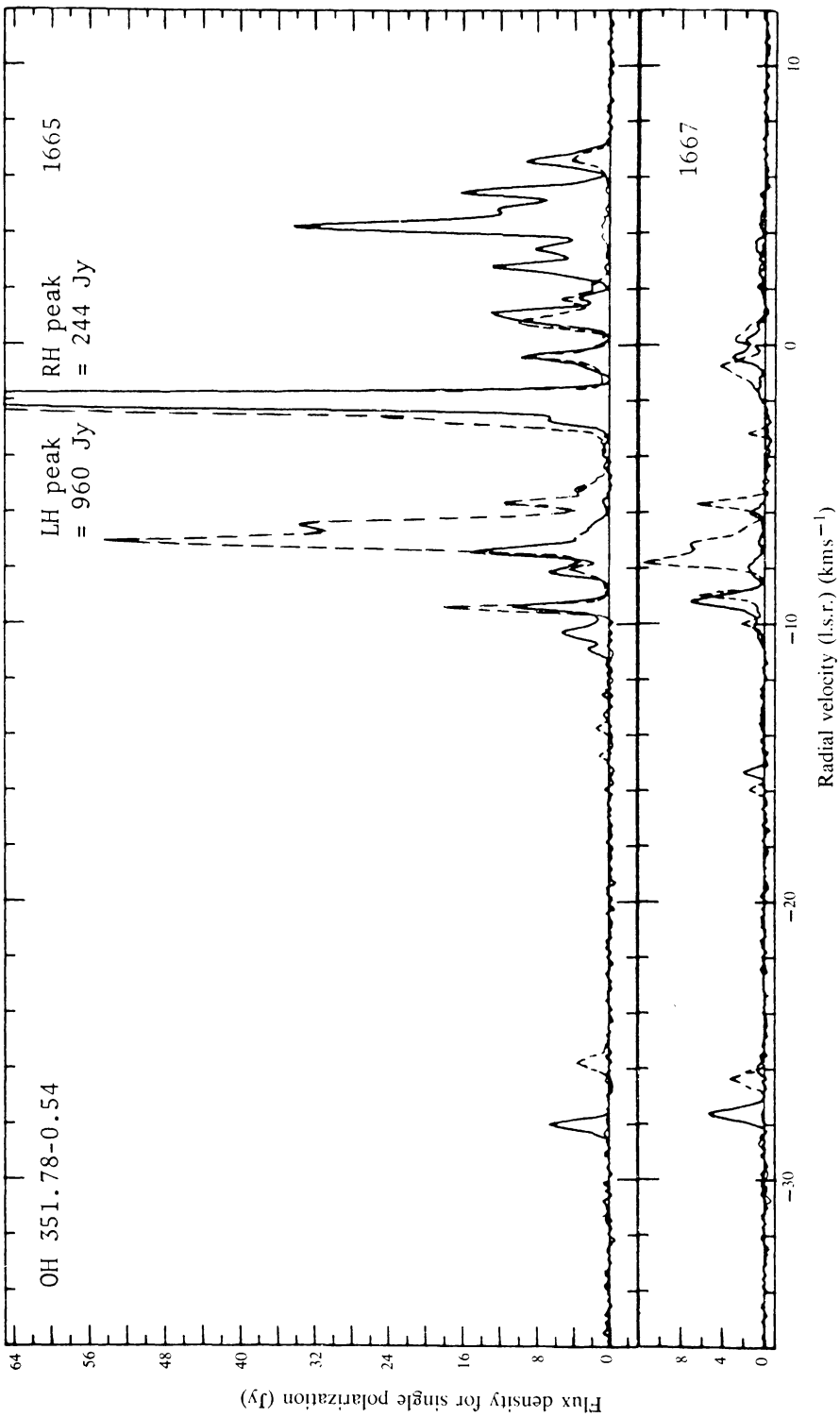

Fig. 13

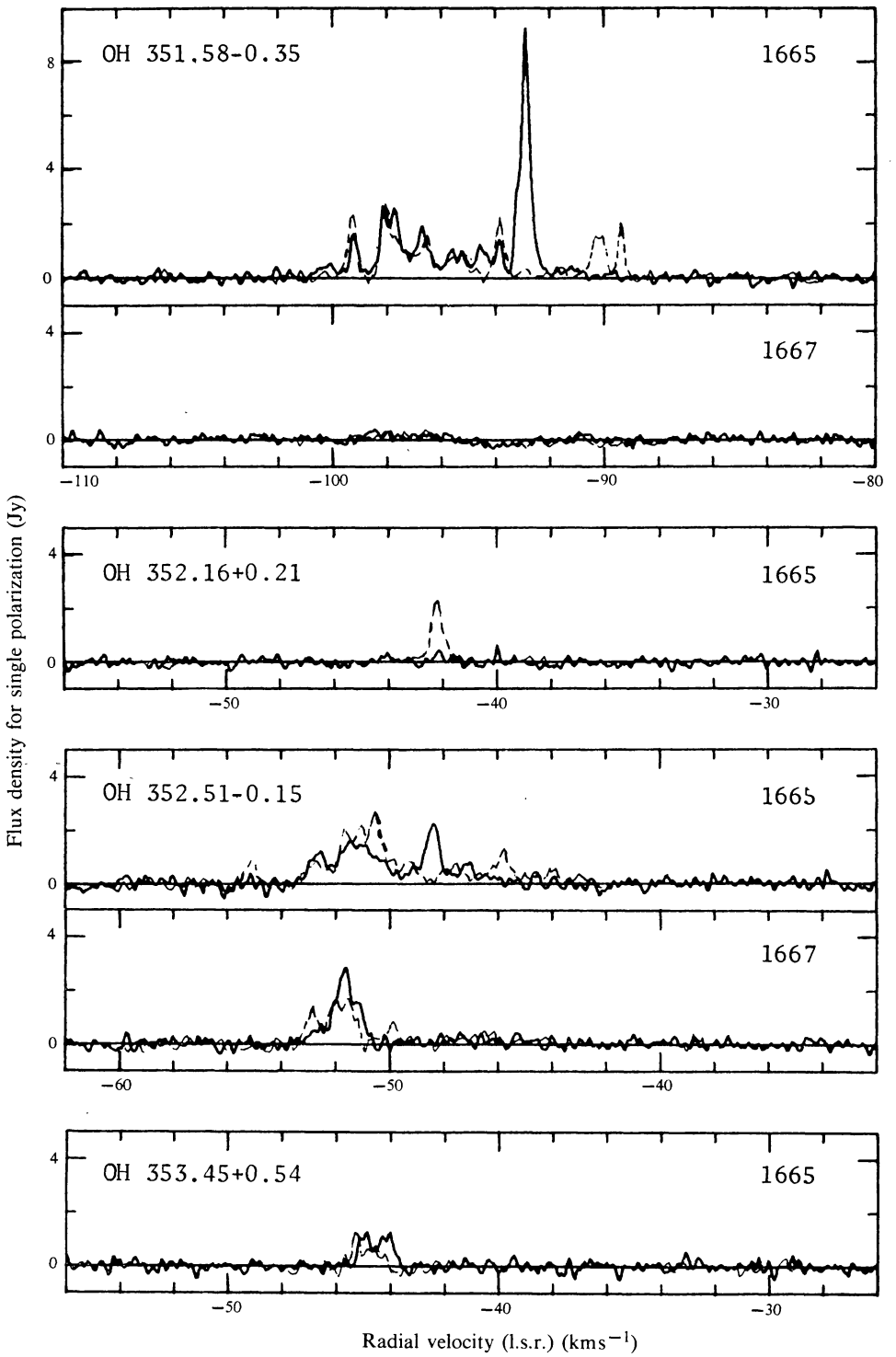

Fig. 14

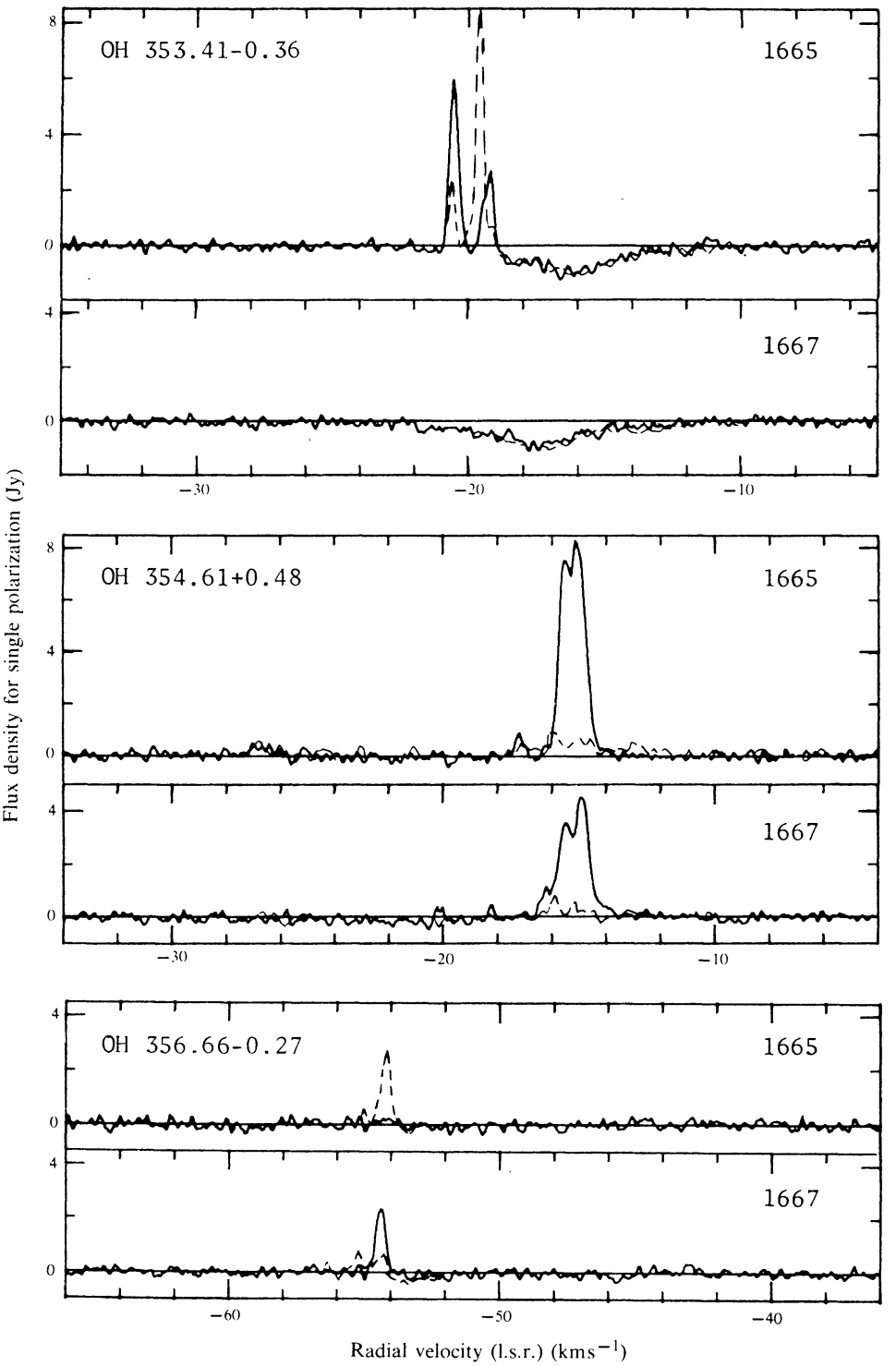

Fig. 15

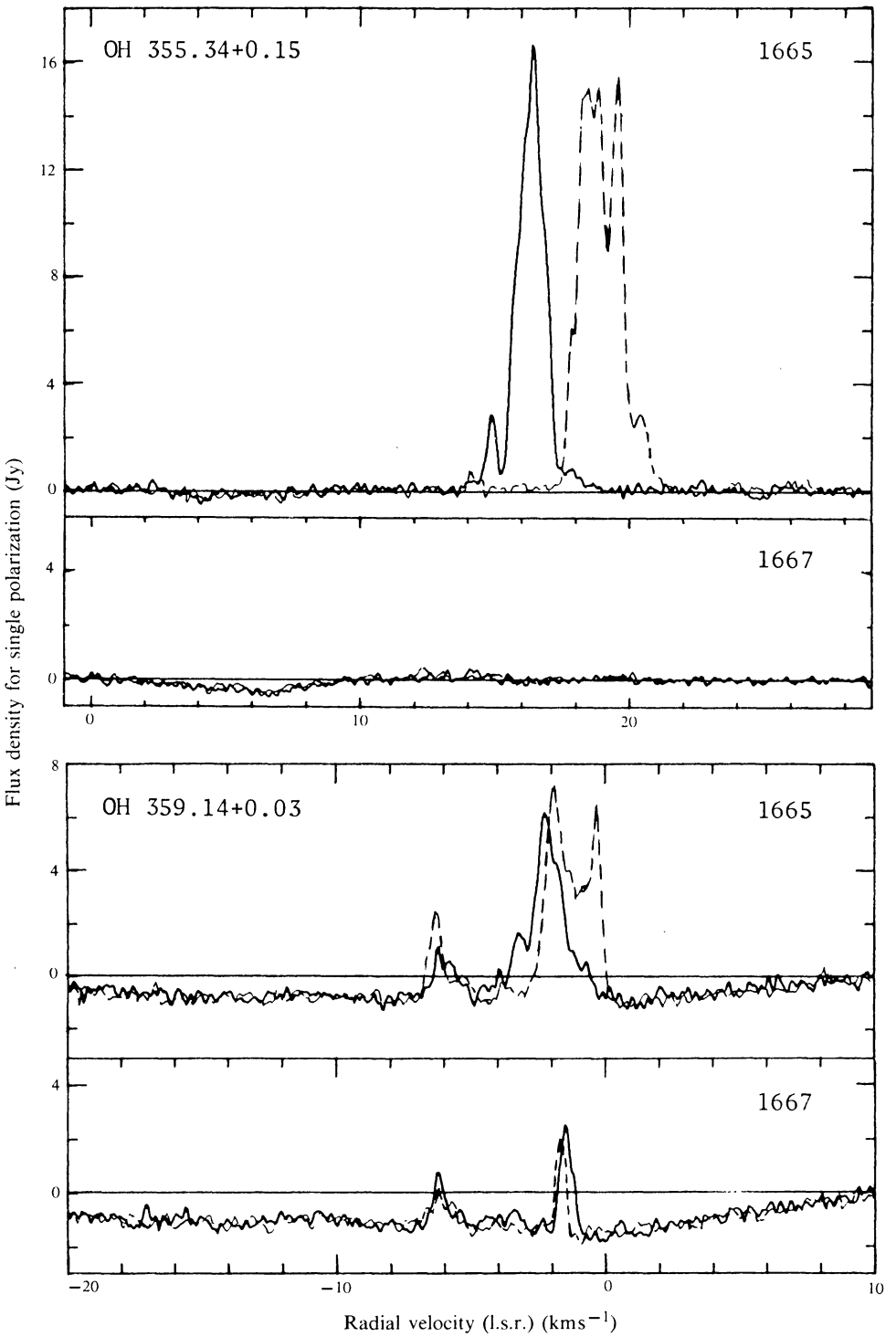

Fig. 16

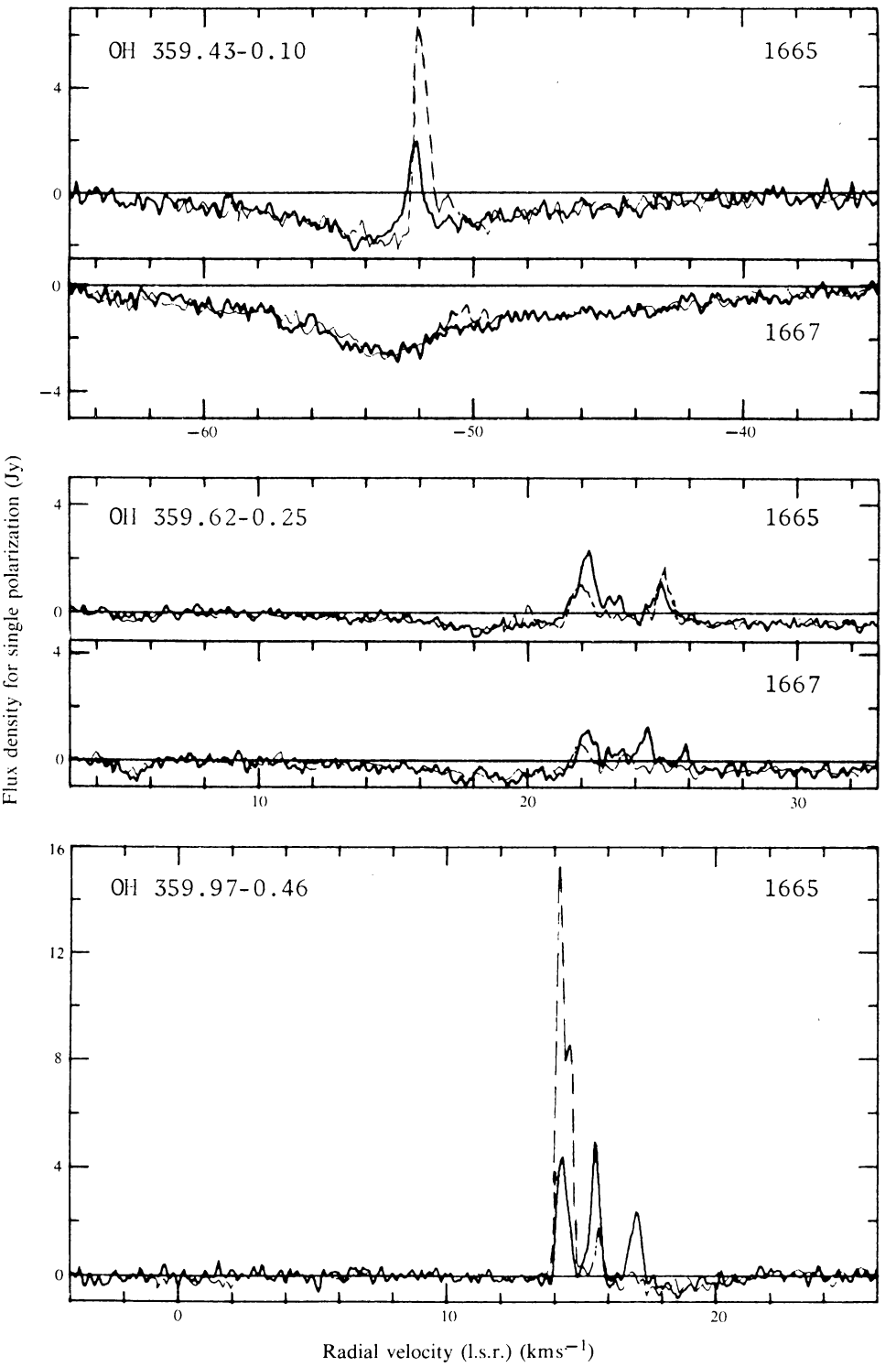

Fig. 17

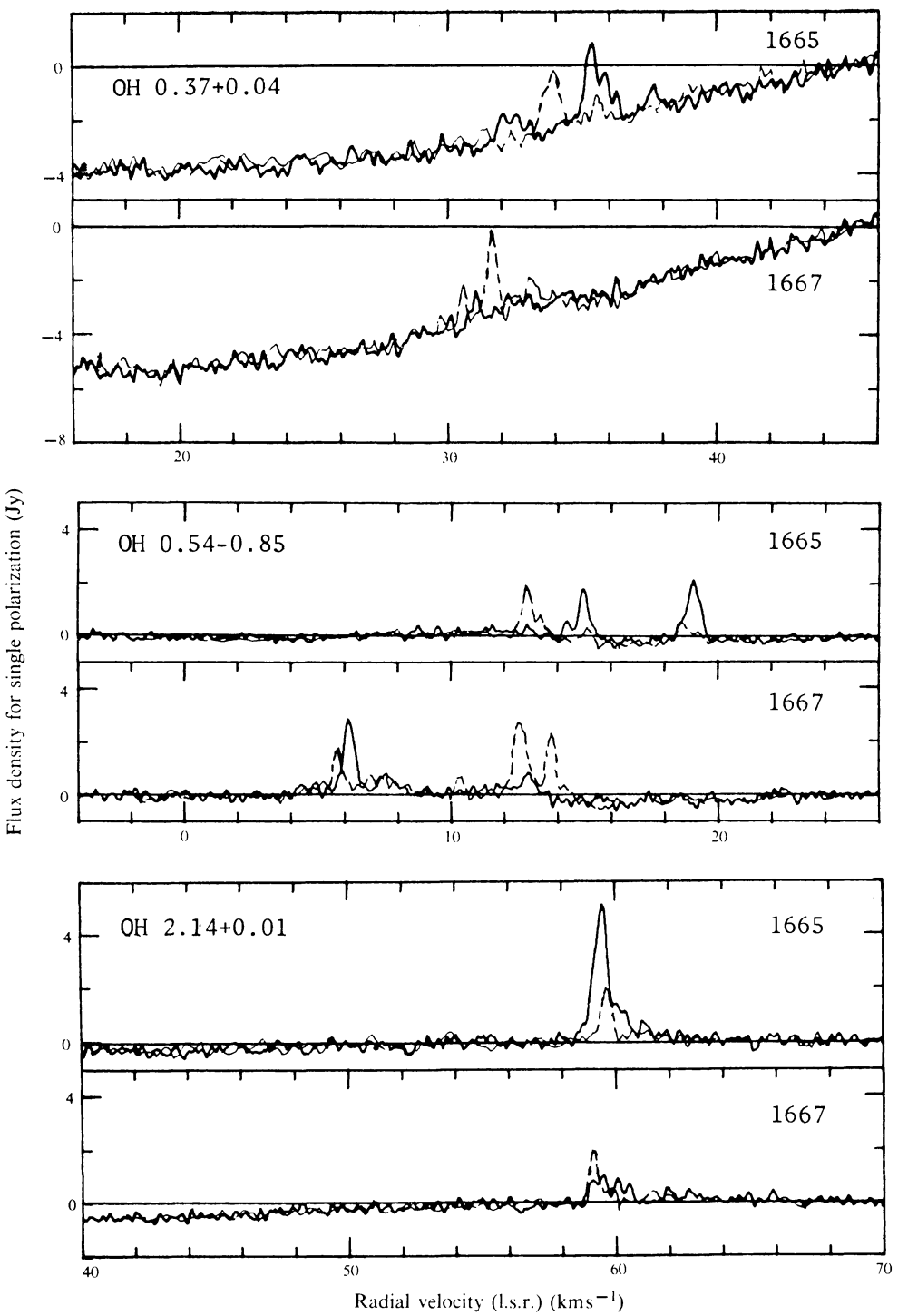

Fig. 18

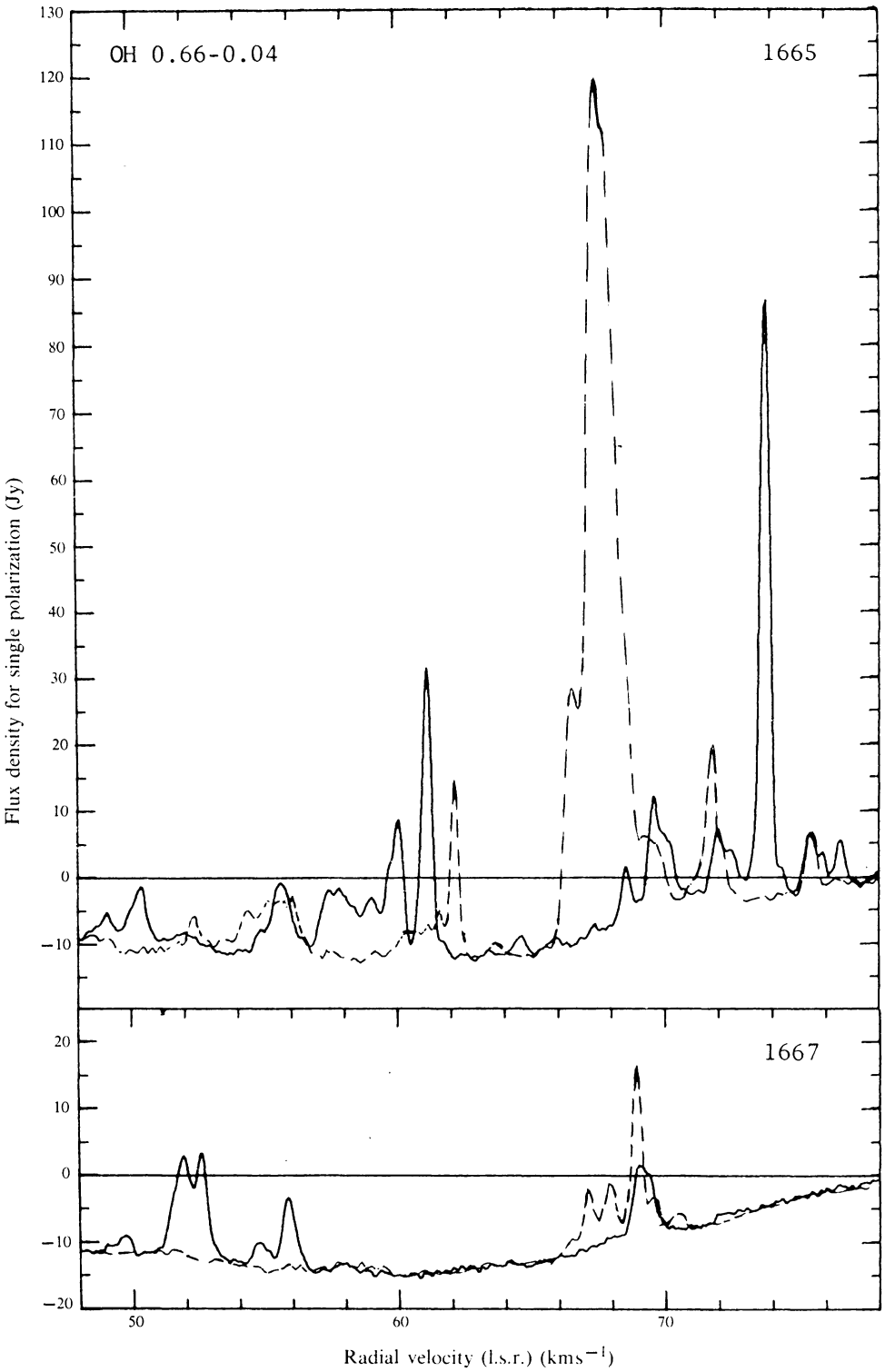

Fig. 19

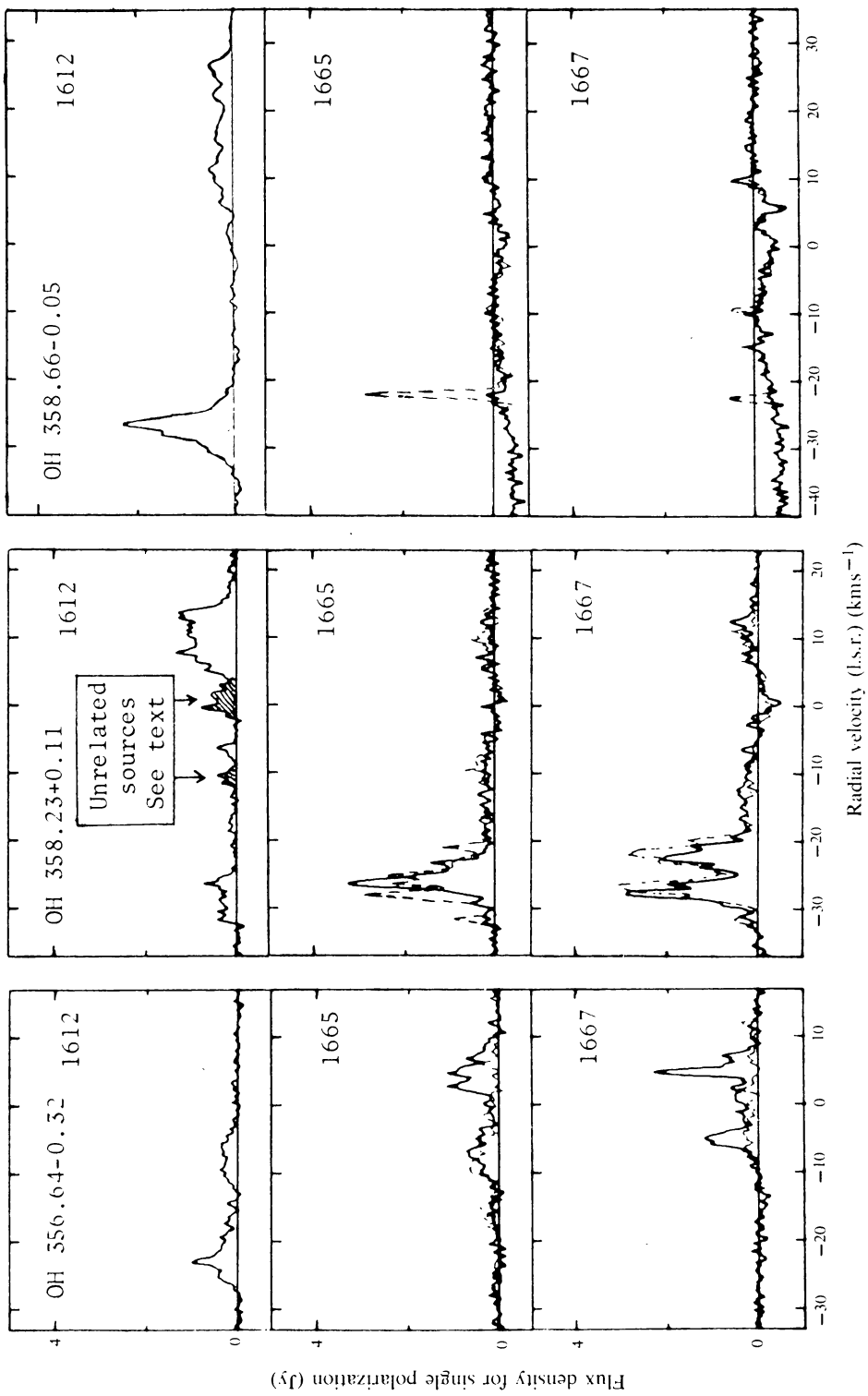

Fig. 20. Spectra of three OH masers that probably are associated with late-type stars. The 1612 MHz profiles show the *average* of RHC and LHC polarization, with the total intensity being twice the plotted value. The velocity resolution is 0·36 km s^{-1} (2 kHz).

OH 345·51+0·35 (*Fig. 6*). This source was discovered by Robinson *et al.* (1974). The major features seen in 1970 at both 1665 and 1667 MHz are still prominent, though with intensities which have varied by factors of up to 2 over the ten-year interval.

OH 345·70−0·09 (*Fig. 7*). Discovered by Robinson *et al.* (1974), the source shows 1665, 1667 and 1612 MHz emission. At 1665 MHz the emission is still similar to that in 1970, although the RHC feature at $v = -8\,\mathrm{km\,s^{-1}}$ has weakened by a factor of 2. At 1667 MHz a considerable increase (by a factor of 3) has occurred in the feature at $v = -7\,\mathrm{km\,s^{-1}}$.

OH 346·48+0·13 (*Fig. 7*). A single feature, 100% LHC polarized, is seen.

OH 347·63+0·15 (*Fig. 8*). Emission is present at 1665, 1667 and 1612 MHz (Robinson *et al.* 1974). The 1665 MHz intensity is currently much stronger than in 1970 but there has been little change at 1667 or 1612 MHz.

OH 347·87+0·01 (*Fig. 7*). The spectrum is dominated by a 100% LHC polarized single feature.

OH 348·55−0·97 (*Fig. 8*). In addition to observing the emission at 1665 and 1667 MHz first reported by Caswell *et al.* (1977), our present investigation covered the 1720 MHz transition and shows emission with two features of opposite circular polarization separated by $\sim 0{\cdot}6\,\mathrm{km\,s^{-1}}$. This may correspond to Zeeman splitting in a line-of-sight magnetic field of 5 mG. No such simple patterns are evident in the 1665 or 1667 MHz emission. In the four years since the measurements of Caswell *et al.* (1977) the 1665 MHz profile has retained the large number of features at the same velocities and sense of polarization, but the intensities have varied by up to a factor of 2. The weaker 1667 MHz emission shows comparable changes.

OH 348·73−1·06 (*Fig. 8*). The spectrum of this source remains generally similar to its appearance when discovered by Caswell *et al.* (1977).

OH 349·07−0·01 (*Fig. 9*). Although this weak source was noted by Turner (1970) and Caswell and Robinson (1974), the present results are the first to provide an accurate position and profile.

OH 349·09+0·11 (*Fig. 9*). The features have varied typically by factors of 2 since the 1970 discovery measurements of Robinson *et al.* (1974); a feature at $v = -90\,\mathrm{km\,s^{-1}}$ is now seen beyond the velocity range covered by the previous observations. Weak 1667 MHz emission is possibly indicated in the present measurements.

OH 350·11+0·09 (*Fig. 10*). This is a strong new source at an unambiguously large distance of nearly 10 kpc; it is thus one of the most intrinsically luminous OH masers known (with a peak intensity of $L = 6000\,\mathrm{Jy\,kpc^2}$).

OH 351·16+0·70 (*Fig. 11*). This is the well-known source often referred to as NGC 6334B or NGC 6334S(outh). At both 1665 and 1667 MHz the features seen a decade ago (Robinson *et al.* 1970) are still recognizable with the same circular polarization but with intensities differing by up to a factor of 3 (at 1665 MHz they are generally weaker now). See Sullivan and Kerstholt (1976) for a history of the variability of this source.

OH 351·41+0·64 (*Fig. 12*). This is the well-known source often referred to as NGC 6334A or NGC 6334N(orth). At both 1665 and 1667 MHz the features seen a decade ago are still recognizable with no great changes in intensity (generally less than a factor of 2, although at 1667 MHz the LHC feature at $-9{\cdot}4\,\mathrm{km\,s^{-1}}$ is now

22 Jy compared with 8 Jy a decade ago). Sullivan and Kerstholt (1976) also remarked on the generally low variability of this source. The 1720 MHz emission likewise shows no major change. The source is one of those most suggestive of Zeeman splitting (Gardner *et al.* 1970), with the same sense and magnitude of magnetic field (5·7 mG) inferred from several OH transitions. Many individual features of the 1665 and 1667 MHz emission seem to be Zeeman doublets, with comparable intensity, suggesting a region with no large *gradients* of magnetic field or velocity.

OH 351·78−0·54 (*Fig. 13*). As we noted earlier (Caswell and Haynes 1980), this source is currently the most intense OH maser in the sky. Our present measurements, with higher velocity resolution than that in our earlier report, show the principal feature to be very narrow in velocity and thus more intense ($\sim$1000 Jy and LHC polarized) than when observed at lower resolution. Spectra obtained with 0·8 kHz resolution on 1980 October 4 and 1981 February 3 (the latter shown in Fig. 13) show no major changes over this four-month period.

In addition to its strikingly large intensity, the source shows an unusually wide spread in velocity of 36 km s^{-1}. The isolated features near $v = -27$ km s^{-1} are strongly suggestive of a 'Zeeman pair' (at both 1665 and 1667 MHz), generated by a magnetic field of 3·7 mG.

There is weak emission at 1612 MHz, probably spatially extended and coextensive with weak 1720 MHz absorption. The radio continuum shows a weak source at 5 GHz of 0·3 Jy which is probably an isolated HII region. No optical emission is visible on the red print of the Palomar Sky Survey (southern extension).

OH 352·16+0·21 (*Fig. 14*). This source is unremarkable, apart from being 100% LHC polarized.

OH 352·51−0·15 (*Fig. 14*). This OH maser lies in the direction of radio continuum and recombination-line emission from an HII region; however, the maser is presumably not related to the HII region since the velocity of the radio recombination line (-82 km s^{-1}) differs markedly from that of the maser.

OH 353·41−0·36 (*Fig. 15*). In addition to 1665 MHz emission, this source shows strong 1720 MHz emission (but no significant 1667 MHz emission). The strongest pair of RHC and LHC polarized features at 1665 MHz are separated by 1·1 km s^{-1}, and the pair of 1720 MHz features are separated by approximately one-fifth of this amount; both separations are compatible with Zeeman splitting in a magnetic field of 1·9 mG. The 1665 MHz emission profile is similar to that of ten years ago, but stronger by a factor of $\sim$2.

OH 353·45+0·54 (*Fig. 14*). The 1665 MHz emission is confined to the small velocity range -43 to -46 km s^{-1}; no 1667 MHz emission was detected but 1612 MHz emission is present in the velocity range -36 to -40 km s^{-1}. In view of this velocity offset, further measurements are needed to ascertain whether the 1612 MHz emission is at *precisely* the same position as the 1665 MHz maser. No 1720 MHz absorption is present so the 1612 MHz emission is unlikely to be an extended type IIc source.

OH 354·61+0·48 (*Fig. 15*). Both 1665 and 1667 MHz emission profiles are nearly 100% RHC polarized and show identical double-peaked velocity structure, with the 1665 MHz intensity being stronger by a factor of $\sim$2. Weaker emission is present at 1612 MHz.

OH 355·34+0·15 (*Fig. 16*). This maser has shown essentially no change over a ten-year period (Caswell and Robinson 1974). As noted by Caswell and Robinson, the separation of RHC and LHC components may be due to Zeeman splitting in a field of 4·5 mG. Weak emission is probably present on our 1667 MHz profile. The maser coincides with a continuum radio source possibly associated with a very extended faint optical HII region (sometimes referred to as NGC 6383, although this is strictly a star cluster within the nebula). The velocity of both the OH maser and the radio recombination line is positive, which on a strict galactic rotation model would imply a distance somewhat exceeding 20 kpc, at which distance the intrinsic luminosity of the maser would make it the third strongest known. More likely the source is closer than 2 kpc (a distance compatible with optical emission being visible) and has a somewhat anomalous velocity.

OH 356·64−0·32 (*Fig. 20*). This very unusual source shows emission at 1665, 1667 and 1612 MHz (see Caswell *et al.* 1981). Our position measurements confirm that all three transitions arise from the same position. Emission extends over the quite large velocity range from -28 to $+13$ km s^{-1}, with main-line emission prominent near $v = +5$ km s^{-1} and 1612 MHz emission near $v = -23$ km s^{-1}; all three transitions emit (but slightly less strongly) near the centre of this range, $v \approx -7$ km s^{-1}. The main-line emission is highly polarized and shows several sharp features which have undergone independent intensity variations by up to a factor of 4 over the three-year period during which we have studied them. In contrast, the 1612 MHz emission is less strongly polarized and although variations may be present in the emission as a whole, no sharp features showing independent variations are present. As noted by Caswell *et al.* (1981), there is also an associated H_2O maser with centre velocity of -10 km s^{-1} (Batchelor *et al.* 1980) and the infrared star IRC-30308 seems a likely origin for the maser emission. Lockwood (1974) suggested that this object is an M-type giant but Baudry *et al.* (1977) suggested it is a supergiant. Most likely we are observing a circumstellar shell expanding (or contracting), but the OH emission characteristics differ greatly from most of the OH/IR stars with late M-type (giants, Mira variable or supergiant) identifications.

OH 356·66−0·27 (*Fig. 15*). The emission at 1665 MHz is accompanied by 1667 MHz emission of comparable intensity. Whereas the 1665 MHz emission is almost 100% LHC polarized, the 1667 MHz emission is almost 100% RHC polarized. Such a situation is rare, as most often when a single strongly polarized feature is present on each main line, the two have the same sense of circular polarization.

OH 358·23+0·11 (*Fig. 20*). Emission is strongest at 1665 and 1667 MHz, with accompanying weaker emission at 1612 MHz. At all three frequencies emission is present in two velocity ranges, separated by ~ 45 km s^{-1}. This double-peaked velocity structure, together with significant 1612 MHz emission, is characteristic of the late-type OH/IR stars. R.A.M. Walterbos (personal communication), in a search for OH/IR stars, discovered the 1612 MHz emission independently of our discovery of the stronger main-line emission. The 1612 MHz profile is somewhat confused on account of a (presumably unrelated) type IIc source with $v \approx 0$ km s^{-1} (the main-line absorption and 1720 MHz absorption at this velocity confirm the IIc classification). Further confusion is caused by emission from a nearby OH/IR star OH 358·1+0·1 discovered by Baud *et al.* (1979) which has 1612 MHz emission at

velocities of -40 and -11 km s^{-1}; our data suggest that the Baud *et al.* position estimate for OH 358·1+0·1 of R.A. 17^h 37^m 12^s, Dec. $-30°\,30'$ is too far south, and a better declination estimate is $-30°\,25'$.

The source OH 358·23+0·11 is unusual as an OH/IR star in having main-line emission stronger than 1612 MHz emission. The velocity range showing weaker main-line emission has stronger 1612 MHz emission and vice versa. The 1665 MHz emission changed considerably between 1980 August and 1981 September (the latter is shown in Fig. 20); most notably the LHC feature at $v = -28$ km s^{-1} was not detectable in 1980 August.

OH 358·66−0·05 (*Fig. 20*). This source, discovered by Caswell *et al.* (1981) at 1612 MHz, shows quite strong 1665 MHz emission and somewhat weaker 1667 MHz emission. This main-line emission is highly circularly polarized and variable. A possible identification with IRC-30316 (Caswell *et al.* 1981) seems now to be excluded in view of our confirmation of the radio position with smaller errors, and the indirect confirmation of the IRC position by Hansen and Blanco (1975), which indicates that the maser and the IRC source are separated by more than 90″, greater than the combined position uncertainties. Nonetheless, the double-peaked velocity structure and stronger 1612 MHz emission suggest that the OH maser corresponds to an OH/IR late-type star; thus any IR counterpart is presumably weaker than the IRC source at short IR wavelengths. The strong main-line emission, with its high degree of circular polarization, shows the source to be one of the rarer varieties of OH/IR star, perhaps a supergiant like VYCMa. Dramatic variability of the main lines also resembles that of VYCMa: at 1665 MHz in 1981 September, about seven months after the profile shown in Fig. 1 was observed, the feature at $v = -22$ km s^{-1} had dropped to 0·8 Jy and a new feature (100% LHC polarized) at $v = -9$ km s^{-1} had reached an intensity of 1·2 Jy.

OH 359·14+0·03 (*Fig. 16*). Very broad OH absorption is present in this direction. Whereas for the previous sources the baseline shown is the level of the continuum emission, the baseline for this source (and several sources following) is arbitrary, with the highest level of the profile baseline set to zero. Intensity measurements of the maser are quoted relative to a smoothly interpolated baseline. Note that since the absorption is extended, its depth in units of flux density would decrease for a smaller beam size whereas the maser emission intensity would be unchanged.

OH 359·43−0·10 (*Fig. 17*). This source is situated in a broad absorption dip.

OH 359·62−0·25 (*Fig. 17*). This source is situated in a broad absorption dip.

OH 0·37+0·04 (*Fig. 18*). Note that the sloping 'baseline' is part of a very broad absorption feature.

OH 0·54−0·85 (*Fig. 18*). The main-line emission is accompanied by weak 1612 MHz absorption and weak 1720 MHz (type IIa) emission. Gardner and Whiteoak (1975) reported absorption at both 1612 and 1720 MHz but, with hindsight, it is clear that their 1720 MHz profile was accidentally inverted during data processing. Thus their claim that it showed absorption on both satellite lines yet very little absorption on the main lines, and was thus an exceptional OH cloud, is invalid. Despite its situation in the general direction of the galactic centre, the maser is probably nearby (~2 kpc distant in the Sagittarius arm), as suggested by Gardner and Whiteoak on account of its coincidence with RCW 142, a visible compact HII region, which also shows continuum and recombination-line radio emission.

OH 0·66−0·04 (*Fig. 19*). This is the well-known source Sgr B2. The emission is superimposed on a very broad absorption feature. Most of the 1665 and 1667 MHz emission features reported a decade ago are still recognizable with only small changes of intensity. In particular, comparison with the 1966 May profiles (Palmer and Zuckerman 1967) shows the following: (i) At 1665 MHz all features are still detectable, with intensity changes of less than 30% in most cases; at the intermediate epoch 1969 June (Robinson *et al.* 1970) the features are similar or intermediate in intensity. (ii) At 1667 MHz all features are very similar apart from our new double-peaked feature at $v = +51$ to $+53$ km s^{-1}; surprisingly, the feature at $+56$ km s^{-1} present in the Palmer and Zuckerman profile *and* in our current (1981) profile seemed absent in 1969 May (Robinson *et al.* 1970), but the adjacent feature at $v = +54{\cdot}5$ km s^{-1} was much stronger; all other features of 1969 June were similar to those of 1966 May. (iii) At 1720 MHz the emission is currently somewhat stronger than a decade ago.

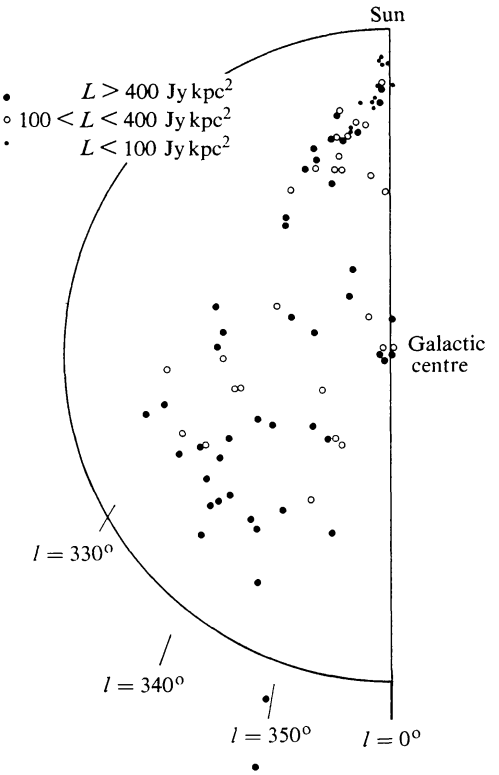

Fig. 21. Distribution of type I OH masers, showing the 85 sources from the present survey and Part I (see Section 3*a* for a discussion of the assignment of distances).

3. Discussion

(*a*) *Distribution of Type I OH Masers in the Galaxy and Their Luminosity Function*

If we accept kinematic distances derived on the assumption of a simple galactic rotation model, we can assign each maser a position in the Galaxy. Fig. 21 shows the observed distribution of all the type I masers from Part I and the present survey (the method by which it was obtained will be discussed later). We can thus characterize the distribution as a function of (i) radial distance from the centre of the Galaxy, (ii) azimuthal angle and (iii) luminosity. The statistics are not sufficient

to investigate all three functional dependences simultaneously and we shall treat them as independent of one another. We can then, with quite good statistics, derive a radial distribution (averaged over luminosity, above some limiting value), and also a luminosity function (averaged over the whole Galaxy).

The data from the present paper combined with the data from Part I yield a sample of 85 type I masers. Our survey has a sensitivity limit of ~ 1 Jy, where this limit refers to the on-source peak intensity measured with high velocity resolution. If we consider sources with intrinsic luminosity ($L = Sd^2$) greater than 400 Jy kpc^2 then we have completeness to a distance d of 20 kpc and thus to a galactocentric radius R of ~ 10 kpc. We assume a Sun to galactic centre distance of 10 kpc and use the Schmidt (1965) model of galactic rotation which (in common with other such models) yields a unique value of R, but an ambiguity in the distance for $R < 10$ kpc. This ambiguity between 'near' and 'far' distances must be resolved in order to assign the correct luminosity to a source; this is clearly necessary in order to derive a luminosity function and (not so obvious) is also necessary to define a luminosity-limited sample in order to investigate the radial distribution in the Galaxy.

In Part I we derived upper and lower limits to the luminosity function by making the alternative assumptions that (with the exception of a few sources whose distances were known) all sources were at the far kinematic distance or all sources were at the near kinematic distance. For the present enlarged sample these extreme alternatives were again explored and clearly neither represents the true distribution:

(1) The first assumption is internally contradictory, since a significant number of sources are expected to be discovered at the near distance (at least one-fifth of the total, because this is roughly the ratio of the volumes covered by near and far distances, and actually greater than one-fifth because the luminosity function extends to weaker sources detectable *only* at the near distance).

(2) The second assumption also proves to be internally contradictory, since it turns out that approximately one-half of the sources have luminosities high enough to be detected at the far distance and thus many *are* presumably detected at the far distance (especially since the far distances occupy a volume of space about four times larger than the near distances).

We may then vary the proportions assumed to be at the near and far distances until there is no internal contradiction. As a reasonable preliminary estimate (which, as we shall see later, ultimately proves to be adequate) we will assume one-half are at the near distance. On average, those with the highest received flux density are likely to be nearest; therefore as a first approximation we assign to the far distance those sources which would lie below the median luminosity if all sources are assumed to be at the far distance. Exceptions were made for the few individual sources for which other evidence contradicted this assumption. Fig. 21 is based on this finally adopted distribution.

Radial Distribution. We first attempt to model the radial distribution, restricting ourselves to sources with $L > 100$ Jy kpc^2 so that our limiting sensitivity of 1 Jy corresponds to completeness out to a distance of 10 kpc, i.e. it reaches to the galactic centre and thus provides data right down to $R = 0$. The sources are first binned in galactocentric annuli of width 1 kpc; to obtain the distribution in the whole Galaxy, the numbers in each annulus were 'corrected' by factors equal to the total area of the annulus (over the whole galactic disk) divided by the portion of the

annulus to which we were above the sensitivity level in the present search. For $R < 6$ kpc, the correction factors are approximately a factor of 2 to allow for searching only one-half of the Galaxy, and there is no heavy reliance on the accuracy of our sensitivity limit. However, for $R > 6$ kpc quite large correction factors are involved in a few instances; thus our results here are more dependent on the precise value of our sensitivity limit and on the statistical errors. Therefore, in the range $5 < R < 9$ kpc, a check on the *relative* numbers of sources in these annuli was made by considering a sample limited to $L > 400$ Jy kpc^2 which does not require any correction factors dependent on limited sensitivity. The agreement was generally good and the finally adopted relative values (of source numbers in adjacent bins) are the mean of the results using the sample limited to $L > 400$ Jy kpc^2 and the sample limited to $L > 100$ Jy kpc^2. However, the absolute values are normalized to correspond to a sample complete above the 100 Jy kpc^2 limit. Table 2 shows the results; the radial density distribution is also plotted as a histogram in Fig. 22.

Table 2. Radial distribution in Galaxy of type I OH masers with $L > 100$ Jy kpc^2

	Galactocentric radius (kpc)									
	0	1	2	3	4	5	6	7	8	9	10
Observed number	5	2	4	6	4	17	19	10	4	1[A]	
'Corrected' number in whole Galaxy	6	2	8	13	10	48	108	75	54	5	
Corrected spatial density in galactic disk (kpc^{-2})	1·91	0·21	0·51	0·59	0·35	1·39	2·64	1·59	1·01	0·08	

[A] To reduce the statistical errors inherent in small numbers, two sources in the region $9 < R < 11$ kpc were averaged.

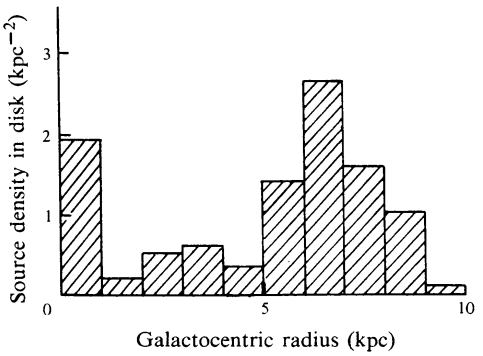

Fig. 22. Histogram showing the spatial density of type I OH masers in the galactic disk as a function of galactocentric radius.

Two tests were made to check that no internal contradictions are present (greater than the statistical uncertainties). Firstly we note that sources assumed to be at the far distance considerably influence the model distribution. Therefore this model distribution will not *necessarily* agree well with the actual spatial distribution of sources at the near distance (where we expect to have a complete sample at the level of 100 Jy kpc^2). The fact that they do agree well (compare Table 2 with Fig. 21) is gratifying and lends confidence to the accuracy of the model. Secondly, for sources with $L > 400$ Jy kpc^2, where we expect to essentially have completeness even at the

far distance (for the sector of galactic disk searched), we find that the number of sources at the far distance compared with those at the near distance is higher, roughly in the ratio of the areas of disk searched, as it should be if the model is to be satisfactory.

A striking feature of our OH maser distribution is the peak near the galactic centre ($R < 1$ kpc). Although apparently based on three sources for which $l < 360°$, this feature is in fact corroborated by two more sources in our list for which l is slightly greater than 0°. There are, of course, well-known problems of assigning kinematic distances to sources near the galactic centre; however, in this direction objects with velocities differing significantly from 0 km s^{-1} are almost certainly located within 1 kpc of the centre since very few comparable objects are found at longitudes only slightly further from the centre. We recall also that there is essentially no correction needed for limited sensitivity out to $R = 6$ kpc. Thus the overall shape, showing a peak at $R < 1$ kpc, followed by a relative dearth of sources and then a sharp rise at $R > 5$ kpc, is quite reliable. It is somewhat less clear how steep the fall-off in spatial density is at large R; the quite large density remaining in the interval $8 < R < 9$ kpc is in fact composed entirely of sources with $8 < R < 8{\cdot}5$ kpc. A practical conclusion resulting from our radial distribution is that the extension of our survey from longitude 326° to 305° might result in the detection of an additional 30 sources despite the relatively low abundance of prominent HII regions here. Such a survey would then improve the estimate of the spatial density at large values of R.

We can also see from Table 2 that our model contains 329 sources with $L > 100$ Jy kpc^2 out to a radius of 10 kpc; the fact that this estimate is based on a total of 73 observed sources in a sector comprising approximately one-third of the galactic disk shows that the estimate depends only weakly on the correction factors which we applied to allow for incompleteness caused by sensitivity limitations. Within $R < 8$ kpc our model has 270 sources, indicating that our preliminary estimate in Part I (250 sources) was quite a good approximation. In the next subsection we consider this from a slightly different viewpoint.

It is interesting to compare our radial distribution for type I OH masers with that of other galactic objects. It shows a general resemblance to the distribution of HII regions and H_2CO absorbing clouds (see e.g. Downes *et al.* 1980) but with a general shift to larger galactocentric radii, i.e. the major concentration lies within $5 < R < 9$ kpc, whereas the distributions of HII regions and H_2CO clouds tend to lie between 4 and 8 kpc. The difference may stem from the fact that our distribution was obtained from southern sources while the others were obtained from northern sources. The HII regions and closely related objects lie in spiral arms rather than circular annuli and, as can be seen from the plot of Georgelin and Georgelin (1976) (see also Downes *et al.* 1980), by chance the major spiral arms seen from the south with $l < 360°$ tend to be further from the centre than those seen from the north with $l > 0°$. In many respects it seems likely that the reliability of the distribution obtained for OH masers is greater than that for the other objects since there are no confusion problems. Some uncertainties which are present, although not dominant sources of error, are caused by the following:

(1) The fact that the small latitude coverage corresponds to a smaller range of galactic height z for nearby sources than for distant sources. This is partly compensated for by our additional searches, specifically in nearby HII regions

that are displaced from the galactic plane. Any warp in the galactic plane would also affect the results but such warps (as indicated by HI observations) are largely confined to $R > 10$ kpc.

(2) The azimuthal dependence of the distribution, resulting from spiral structure, can only be eliminated by complete coverage of the Galaxy.

(3) The sensitivity limit is partly dependent on the background temperature; consequent failure to detect some sources is likely to be most acute near the galactic centre.

(4) The variations of sensitivity across the grid (depending on source position relative to initial grid position) aggravates the uncertainty in specifying a clear sensitivity limit.

(5) Intrinsic variability occurs; however, this will not *systematically* affect the survey.

In any comparison with other distributions it should be made clear that the present distribution is based on kinematic distances for all the sources, assuming that the Sun is located 10 kpc from the galactic centre. Distributions for radio supernova remnants and radio pulsars are tied to kinematic distances for a *sample* of the objects, with the majority linked to this scale by a secondary *relative* distance indicator. Optical distances suggest that the Sun may be only 8·5 kpc from the galactic centre and distributions derived on that basis should perhaps be scaled up by ~20% for comparison with the present results.

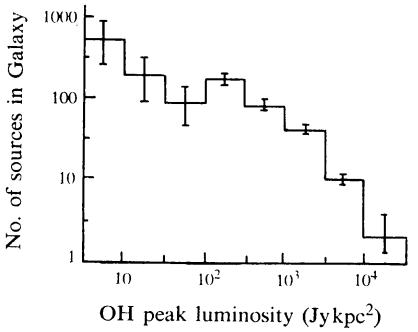

Fig. 23. Luminosity function for OH masers at 1665 MHz, normalized to the total expected in the galactic disk out to the solar distance (assumed to be 10 kpc). The error bars allow only for statistical errors, i.e. $n^{\frac{1}{2}}$, where n is the observed number of sources in each bin.

Luminosity Function. In the previous subsection we grouped together all sources with $L > 100$ Jy kpc^2. In order to obtain a luminosity function we must bin the data in luminosity intervals and sum over all galactocentric radii. We have chosen logarithmic intervals of half a decade (as we also did in Part I) and also extended the investigation to sources with $L < 100$ Jy kpc^2, although of course the larger uncertainties should be especially borne in mind at these low luminosities. Furthermore, at these low luminosities all values of R are not sampled (i.e. weak sources are detectable only near the Sun, near $R \approx 10$ kpc); in order to 'correct' the number to correspond with the distribution over the whole Galaxy, the radial distribution derived for strong sources was assumed valid. In fact there are some merits in assuming this smooth radial distribution for all luminosities rather than retaining the observed annular distributions and summing them. Therefore we tried both approaches, and an arithmetic mean of the numbers in each luminosity bin is used in our final result, shown in Fig. 23. Note that the numbers correspond to the whole

galactic disk area out to $R = 10$ kpc; above $L = 100$ Jy kpc^2, the total is 312 sources, in satisfactory agreement with the estimate of 329 derived in the previous subsection. A monotonic increase in numbers of sources with decreasing luminosity is seen from $L = 3 \times 10^4$ Jy kpc^2 down to 100 Jy kpc^2 and is quite reliably determined; the trend *may* extend to the weakest sources but we cannot be confident of this with the present data sample. Our present luminosity function is compatible with our previous estimate (of Part I) but supersedes it. Note that our preferred assignment of apparently weak sources to far distances and the strongest sources to near distances tends to concentrate the sources in the middle range of luminosity and underestimate the tails of the distribution.

(*b*) *Relative Intensities of the Four Ground-state Transitions*

Although the initial search observations of the present survey were made only on the 1665 MHz transition (with 1667 MHz observations being made only at the positions of detected sources) the main-line (1665 and 1667 MHz) data of the present survey corroborate the conclusions of Part I (conducted on both main lines).

In Part I we found that in 36 out of 40 instances the emission at 1665 MHz was stronger than at 1667 MHz; a similar ratio is found in the present sample of 45 additional type I sources, which has 39 of the sources stronger at 1665 MHz. The ratio of intensity at 1665 MHz to that at 1667 MHz had a median value of ~ 3 for the sources in Part I; the median of the present sample is very similar and the large range of the intensity ratios (~ 80 to $\frac{1}{4}$) is also quite similar to that of Part I.

Narrow-band maser emission on one of the satellite lines (1612 and 1720 MHz) accompanies the main-line emission in 15 of the sample of 85 type I sources obtained by combining the present data with that of Part I. A marked difference in the statistics of Part I and those of the present survey taken individually is apparent and can be attributed to the small numbers involved. Thus, in Part I we found six masers at 1612 MHz and none at 1720 MHz, whereas in the present survey we find six masers at 1720 MHz and three at 1612 MHz. Thus, it now seems that maser emission on the two satellite lines accompanying type I masers may occur with roughly equal probability.

Weak extended emission at either 1612 MHz (type IIc) or at 1720 MHz (type IIa) was extensively discussed by Caswell and Haynes (1975) and Haynes and Caswell (1977). Associated with type IIc emission we commonly find 1720 MHz absorption which is anomalously strong relative to the main lines; likewise, anomalously strong 1612 MHz absorption commonly accompanies type IIa emission. The occurrence of these weak satellite line features in the direction of some type I masers is indicative of quite extended molecular clouds.

(*c*) *Polarization Characteristics*

In the individual notes on sources in Section 2 we remarked on polarization patterns suggestive of Zeeman splitting. An absence of Zeeman pairs, yet with both 1665 and 1667 MHz showing a high degree of circular polarization, predominantly in the same sense, is found in some sources, and this may be indicative of strong gradients of magnetic field and velocity (see Part I).

For the satellite lines the Landé splitting factor is smaller than for the main lines; it is therefore less usual for lines to be split by many times their width (with consequent

loss of one component if gradients of magnetic field and velocity are present); usually either simple Zeeman pairs are seen, or unpolarized emission if there is no 'splitting' greater than the line width.

We should emphasize that the high degree of circular polarization often encountered does not preclude significant linear polarization. Indeed, early measurements (e.g. Robinson *et al.* 1970) showed much linear polarization among the relatively few sources then known. However, with the large increase in the number of sources now known, the systematic measurement of linear polarization will require a very extensive program of time-consuming observations, and this has not yet been possible.

(*d*) *Velocity Structure*

The source OH 340·78−0·10 shows a velocity structure suggestive of a shell in which we see the front and back sides expanding (or contracting), as is common in the late-type stars (see Caswell *et al.* 1981). In this and many other sources of our sample, the major cause of the 'velocity spread' must indeed be general motions in the source rather than Zeeman splitting. The very strong source OH 351·78−0·54 shows a particularly wide velocity spread which must result from large-scale motions.

In this context it is interesting to compare our results with conclusions reached concerning W 3(OH) and W 75N as a result of long-baseline interferometer maps (Reid *et al.* 1980; Norris and Booth 1981; Haschick *et al.* 1981). Reid *et al.* argued that the major cause of the 'velocity spread' in W 3(OH) is Zeeman splitting and that they are only seeing material on the near side of a contracting shell. Clearly, such a model is not applicable to many of the sources in our sample. In the case of W 75N, Haschick *et al.* argued that the maser components reside in a rotating disk and the velocity spread of $\sim 10\ \mathrm{km\,s^{-1}}$ is dominated by this rotation. Testing the applicability of such a model to our sources must in most cases await Southern Hemisphere VLBI maps.

(*e*) *Association with H_2O Masers*

In column 10 of Table 1 we note the results of a search for H_2O masers in the direction of the OH masers. Positive detections were made at 40 of the 49 OH positions. This very high proportion reflects the increased sensitivity of the H_2O searches now being conducted; for a discussion of the implications of this almost 1 : 1 correspondence, in conjunction with a detailed presentation of the H_2O results and consideration of the sensitivity limits, see Caswell *et al.* (1983, present issue p. 401).

(*f*) *Variability*

Variability of the OH masers known for many years is commented on in the notes to the sources (see Section 2). However, many of the masers are new discoveries and our observations provide only first-epoch data.

4. Conclusions

This survey has more than doubled the number of well-observed type I OH masers; most conclusions of Part I are reinforced and here we indicate the main new ones. The increased statistics are especially valuable in relation to the small proportion

showing satellite-line emission, and it now appears that roughly 10% of type I masers have accompanying 1612 MHz maser emission with a slightly smaller (and completely different) fraction showing 1720 MHz emission. It will be important to see how closely related the main-line and satellite-line masers are, and accurate interferometer positions are needed for this. As yet it is unclear whether any other distinguishing properties are correlated with the accompaniment of satellite-line emission. We intend to study these satellite-line masers in a subsequent paper.

The extension of our present survey to the galactic centre has permitted the first reliable estimate of the distribution of masers throughout the Galaxy. A peak in the spatial density between galactocentric radii 5 and 9 kpc is in broad agreement with that of HII regions, although more detailed comparisons await further work on *southern* HII regions in view of an asymmetry between the halves of the Galaxy. The secondary peak in spatial density at the galactic centre is an interesting feature which also shows some correspondence with the HII region distribution; both facts indicate that star formation is still in progress close to the centre, despite a generally low rate at radii less than 5 kpc.

There is some indication that the spatial density of type I masers may remain quite high nearly out to the solar circle and we propose to extend our survey to investigate this further.

References

Batchelor, R. A., Caswell, J. L., Goss, W. M., Haynes, R. F., Knowles, S. H., and Wellington, K. J. (1980). *Aust. J. Phys.* **33**, 139.

Baud, B., Habing, H. J., Matthews, H. E., and Winnberg, A. (1979). *Astron. Astrophys. Suppl.* **35**, 179.

Baudry, A., Le Squeren, A. M., and Brillet, J. (1977). *Liège Astrophys. Colloq.* **21**, 259.

Caswell, J. L., Batchelor, R. A., Forster, J. R., and Wellington, K. J. (1983). *Aust. J. Phys.* **36**, 401.

Caswell, J. L., and Haynes, R. F. (1975). *Mon. Not. R. Astron. Soc.* **173**, 649.

Caswell, J. L., and Haynes, R. F. (1980). IAU Circular No. 3509.

Caswell, J. L., Haynes, R. F., and Goss, W. M. (1977). *Mon. Not. R. Astron. Soc.* **181**, 427.

Caswell, J. L., Haynes, R. F., and Goss, W. M. (1980). *Aust. J. Phys.* **33**, 639.

Caswell, J. L., Haynes, R. F., Goss, W. M., and Mebold, U. (1981). *Aust. J. Phys.* **34**, 333.

Caswell, J. L., and Robinson, B. J. (1974). *Aust. J. Phys.* **27**, 597.

Cohen, R. J., and Few, R. W. (1976). *Mon. Not. R. Astron. Soc.* **176**, 495.

Downes, D., Wilson, T. L., Bieging, J., and Wink, J. (1980). *Astron. Astrophys. Suppl. Ser.* **40**, 379.

Gardner, F. F., Ribes, J.-C., and Goss, W. M. (1970). *Astrophys. Lett.* **7**, 51.

Gardner, F. F., and Whiteoak, J. B. (1975). *Mon. Not. R. Astron. Soc.* **171**, 29P.

Georgelin, Y. M., and Georgelin, Y. P. (1976). *Astron. Astrophys.* **49**, 57.

Hansen, D. L., and Blanco, V. M. (1975). *Astron. J.* **80**, 1011.

Haschick, A. D., Reid, M. J., Burke, B. F., Moran, J. M., and Miller, G. (1981). *Astrophys. J.* **244**, 76.

Haynes, R. F., and Caswell, J. L. (1977). *Mon. Not. R. Astron. Soc.* **178**, 219.

Haynes, R. F., Caswell, J. L., and Goss, W. M. (1976). *Proc. Astron. Soc. Aust.* **3**, 57.

Haynes, R. F., Caswell, J. L., and Simons, L. W. J. (1978). *Aust. J. Phys. Astrophys. Suppl.* No. 45.

Lockwood, G. W. (1974). *Astrophys. J.* **192**, 113.

McGee, R. X., Robinson, B. J., Gardner, F. F., and Bolton, J. G. (1965). *Nature* **208**, 1193.

Norris, R. P., and Booth, R. S. (1981). *Mon. Not. R. Astron. Soc.* **195**, 213.

Palmer, P., and Zuckerman, B. (1967). *Astrophys. J.* **148**, 727.

Reid, M. J., Haschick, A. D., Burke, B. F., Moran, J. M., Johnston, K. J., and Swenson, G. W. (1980). *Astrophys. J.* **239**, 89.

Robinson, B. J., Caswell, J. L., and Goss, W. M. (1974). *Aust. J. Phys.* **27**, 575.

Robinson, B. J., Goss, W. M., and Manchester, R. N. (1970). *Aust. J. Phys.* **23**, 363.

Schmidt, M. (1965). *In* 'Galactic Structure' (Eds A. Blauuw and M. Schmidt), p. 513 (Univ. Chicago Press).
Sullivan, W. T., and Kerstholt, J. H. (1976). *Astron. Astrophys.* **51**, 427.
Turner, B. E. (1970). *Astrophys. Lett.* **6**, 99.
Turner, B. E. (1979). *Astron. Astrophys. Suppl.* **37**, 1.
Weaver, H., Williams, D. R. W., Dieter, N. H., and Lum, W. T. (1965). *Nature* **208**, 29.

Manuscript received 1 October, accepted 29 November 1982